11

Translational dynamics and quantum coherence

In all that we have encountered so far, the evolution of spin phase under the effect of magnetic field gradients has been considered to arise from single-quantum coherence, that simple classical transverse magnetisation generated when the ensemble of nuclear spins is disturbed from thermal equilibrium by a resonant RF pulse. But, as we learned in Chapters 3 and 4, terms in the spin Hamiltonian bilinear in the spin operator can act to transform such magnetisation into various states of quantum coherence. Such terms include homo- and heteronuclear scalar couplings, dipolar interactions and quadrupolar interactions. All are capable of generating double-quantum coherence or, for two-spin interactions, zero-quantum coherence, and—given sufficient spin couplings or in the case of quadrupole interactions, sufficient single-spin quantum number, I—states of n-quantum coherence, where $n > 2$. Once created, these will evolve in phase under the influence of the Zeeman interaction at n times that of the single-quantum state. By such means, sensitivity to magnetic field gradients may be enhanced.

Moving from single to n-quantum coherence changes none of the physics encountered so far. The use of multiple-quantum coherence as a vehicle for imprinting phase information arising from translational dynamics merely represents a tool for amplifying the apparent magnetogyric ratio or gradient amplitude. And of course, as with all enticing tricks, there may be a price to be paid. With what efficiency can we transform our initial magnetisation to a state of multiple-quantum coherence, and then reconvert to the single-quantum state required by our detector? What are the relaxation rates associated with higher quantum coherence, and if faster, will we lose too much signal during coherence preparation, evolution, and reconversion? In short, are the signal-to-noise ratio costs worth the heightened phase-shift sensitivity? While each case must be evaluated on its own merits, we will see that there are systems where the gains are indeed real.

There is another sense in which differing quantum states of the spin system can be enlisted to enhance sensitivity to translational dynamics. A fundamental limit to PGSE NMR concerns the time over which a ensemble phase coherence can be preserved: the maximum value of Δ over which it is possible to observe molecular translation. Conventional wisdom suggests that the best way to maximise the time is to use a stimulated echo, so that the limiting timescale is determined by T_1 relaxation during z-storage. But in fact longer-lived states of spin coherence are possible, in particular certain specially prepared singlet states. In this chapter we will see how such states may be generated and utilised to stretch our time window.

Translational Dynamics and Magnetic Resonance, First Edition, Paul T. Callaghan, © Paul T. Callaghan 2011.
Published in 2011 by Oxford University Press.

Finally, we will encounter a curious aspect of quantum coherence in which diffusion plays an inherent role in determining the signal observed. In liquids, intra-molecular dipolar interactions between spins are motionally averaged to zero by the rapid rotational tumbling of the host molecule. What then of inter-molecular dipolar interactions between spins on different molecules? Here we might hope that translational diffusion acts to cause pairs of molecules to undergo a migrational dance, in which the internuclear vectors between their respective spins will reorient sufficiently rapidly to average these interactions as well. And indeed, if the molecules are sufficiently close, the dance suffices. But as molecular separation increases, the time taken for translational diffusion to permit an orbit in which the vectors sample all possible directions will diverge.

Of course, the strength of the dipolar interactions drops with separation distance r as r^{-3}, so that we might expect these more distant molecular neighbours to impose unaveraged dipolar interactions too weak to matter. But now we face the vastly increasing number of that outer pool of neighbours as we integrate their contributions out to the limits of our sample. A logarithmic divergence presents itself, and what we find is that a residual inter-molecular dipolar interaction persists, with a size determined by two primary factors. The first is the least separation distance, where translational diffusion is no longer capable of dancing away the dipolar interaction. The slower the diffusion, the tighter that inner radius, and the stronger the dipolar contribution. The second factor concerns symmetry. The inner volume determined by the diffusion limit is essentially a sphere, and as we integrate contributions out to the limits of our sample, we do so in spherical shells, so that whatever our sample shape, the effects die away before such shape is capable of breaking spherical symmetry, a symmetry that sums all dipolar contributions to zero. To observe the intermolecular dipolar sum, we need to externally break that spherical symmetry by manipulating the bulk magnetisation phase, and this we may do by imposing magnetic field gradient pulses.

These remarkable intermolecular dipolar interactions were first observed in helium-3 NMR [1], then rediscovered in proton NMR, fully explained and brought to the attention of the wider magnetic resonance community by Warren and co-workers [2–7]. The cumulative interaction strengths are small, on the order of hertz or tens of hertz, but they increase with increasing polarising field strength and decreasing diffusion coefficient, and they particularly appear when magnetic field gradients are applied. For that reason alone we need to understand them. Furthermore, these effects have potential applications in NMR microscopy, in which a subtle interplay of long-range dipolar correlations allow inferences regarding sample internal structure.

11.1 Diffusion measurement using multiple-quantum coherences

11.1.1 Use of dipolar couplings

The first demonstrations of diffusion measurement using multiple-quantum coherences employed the dipolar interaction to convert from the the single-quantum state [8, 9]. Martin *et al.* [8] used double-quantum coherence to measure the diffusion coefficient of dichloromethane (CH_2Cl_2) dissolved at $< 10\%$ concentration in thermotropic liquid crystals in which the nematic order of the host induced a dipolar splitting of several

kilohertz, while Zax and Pines measured the diffusion of benzene dissolved in liquid crystals at higher concentration, using various quantum orders.

As we have seen in Chapter 4, the dipolar interaction between a pair of spins, i and j, involves a bilinear spin operator $\omega_{ij}[3I_{iz}I_{jz} - \mathbf{I_1} \cdot \mathbf{I_2}]$, where ω_{ij} is the 'dipolar precession frequency'. Suppose we start with an equilibrium longitudinal magnetisation represented by a density matrix proportional to $I_{iz} + I_{jz}$. After a 90° RF pulse, the evolution after time t can be described by

$$\begin{aligned} I_{iz} + I_{jz} & \\ & \xrightarrow{-(\pi/2)(I_{ix}+I_{jx})} \quad I_{iy} + I_{jy} \\ & \xrightarrow{3\omega_{ij}I_{iz}I_{jz}} \quad (I_{iy} + I_{jy})\cos\phi - (2I_{ix}I_{jz} + 2I_{iz}I_{jx})\sin\phi \end{aligned} \tag{11.1}$$

where $\phi = \frac{3}{2}\omega_{ij}t$. Only the density matrix term $(I_{iy} + I_{jy})$ is directly observable using Faraday detection, and so the transverse magnetisation detected in our receiver coil is modulated by $\cos(\frac{3}{2}\omega_{ij}t)$, corresponding to two spectral components at frequencies $\pm\frac{3}{2}\omega_{ij}$. This doublet is split by angular frequency $3\omega_{ij}$. Note that the term $\mathbf{I_1} \cdot \mathbf{I_2}$ commutes with the operator $I_{iy} + I_{jy}$, and as for the scalar coupling when the chemical shift is zero, produces no observable interaction.

RF and gradient pulse scheme

To see how RF pulses may be used to create a state of double-quantum coherence from the two-spin dipolar interaction, consider the following sequence of two identical 90° excitations.

$$\begin{aligned} I_{iz} + I_{jz} & \\ & \xrightarrow{-(\pi/2)(I_{ix}+I_{jx})} \quad I_{iy} + I_{jy} \\ & \xrightarrow{3\omega_{ij}I_{iz}I_{jz}} \quad (I_{iy} + I_{jy})\cos\phi - (2I_{ix}I_{jz} + 2I_{iz}I_{jx})\sin\phi \\ & \xrightarrow{-(\pi/2)(I_{ix}+I_{jx})} \quad -(I_{iz} + I_{jz})\cos\phi - (2I_{ix}I_{jy} + 2I_{iy}I_{jx})\sin\phi \end{aligned} \tag{11.2}$$

For $\phi = (2p+1)\frac{\pi}{2}$ where $p = 0, 1, 2...$, we have a transfer to $(2I_{ix}I_{jy}+2I_{iy}I_{jx})$, a state of double-quantum coherence. For a spectral splitting $\Delta\nu$ in hertz, the simple case $p = 0$ corresponds to a time delay between the two RF pulses of $(2\Delta\nu)^{-1}$. Note that higher-order spin couplings (3-spin, 4-spin) can lead to higher orders of coherence. These will arise from different coupling strengths and hence may be generated over longer times with lower efficiency. For the moment, however, we will consider a sequence optimised for double-quantum generation and focus solely on $n = 2$.

Using the spherical tensor language of Table 3.8 and Section 3.4.4, $I_{iy} + I_{jy}$ or $T_{11}(10, s) + T_{11}(01, s)$ evolves under the influence of $T_{20}(11)$ to generate $T_{22}(11) - T_{2-2}(11)$, a superposition of +2QC and -2QC. Note that $[T_{2\pm2}(11), T_{20}(11)] = 0$. Once created, the state of double-quantum coherence is invariant under the effect of the dipolar interaction. This means that it is not subject to dephasing as a result of

an inhomogeneous distribution of dipolar terms. However, it does precess about any Zeeman term in the spin Hamiltonian, such as is imposed by a magnetic field gradient pulse. And it does so at twice the Larmor frequency, since the commutator yields

$$[\omega_0 \left(T_{10}(10) + T_{10}(01)\right), T_{2\pm2}(11)] = \pm 2\omega_0 T_{2\pm2}(11) \tag{11.3}$$

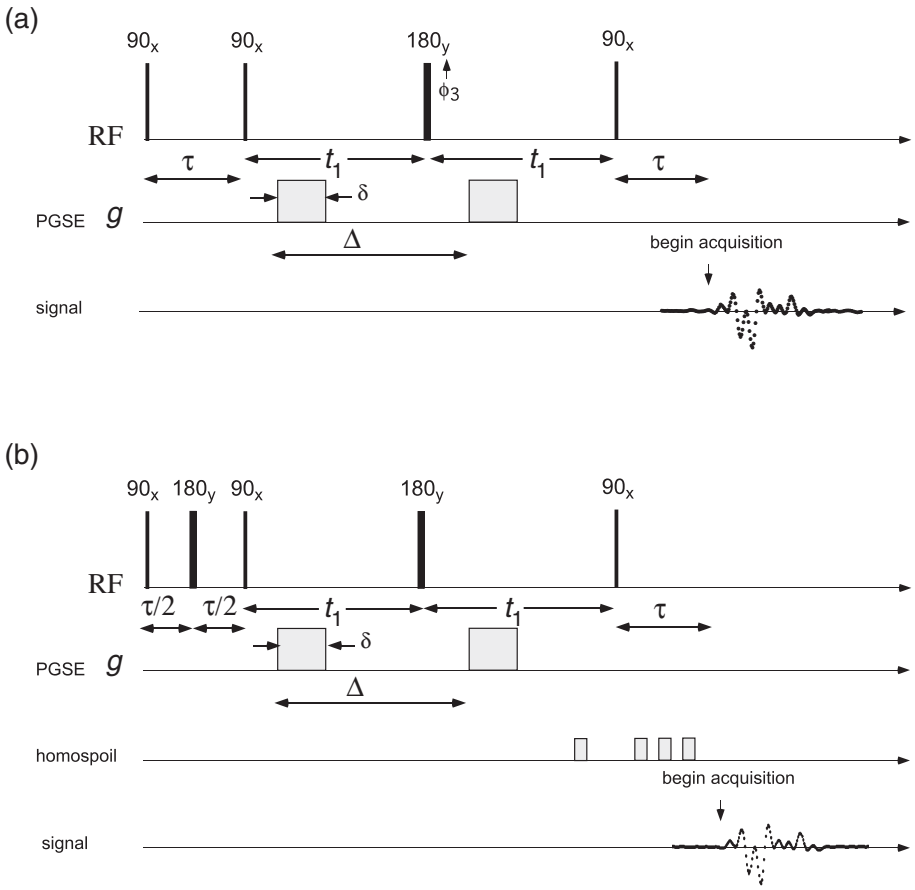

Fig. 11.1 (a) double-quantum spin-echo sequence for diffusion measurement. The final 90° RF pulse at the double-quantum echo transfers coherence from $(2I_{ix}I_{jy} + 2I_{iy}I_{jx})$ to $(2I_{ix}I_{jz} + 2I_{iz}I_{jx})$, which subsequently evolves under the dipolar interaction to observable transverse magnetisation at time τ later. The RF pulses are phase cycled to optimise for coherence selection. (Adapted from reference [8].) (b) Another version of the pulse sequence in which a $90^\circ - 180^\circ - 90^\circ$ echo is used in the initial evolution, refocusing chemical shift or field inhomogeneity, but leaving the dipolar evolution unchanged, and in which homospoil gradient pulses are used to select only those pathways involving n-quantum coherence during the echo periods, T. (Adapted from Zax and Pines [9].)

The double-quantum superposition state, $T_{22}(11) - T_{2-2}(11)$, evolves under the Zeeman Hamiltonian, $\omega_0(I_{iz} + I_{jz}) = \omega_0 \left(T_{10}(10) + T_{10}(01)\right)$, as

$$\begin{aligned} T_{22}(11) - T_{2-2}(11) & \\ & \xrightarrow{\omega_0(I_{iz}+I_{jz})} (T_{22}(11) - T_{2-2}(11)) \cos 2\omega_0 t \\ & \qquad +i(T_{22}(11) + T_{2-2}(11)) \sin 2\omega_0 t \\ & = \quad (2I_{ix}I_{jy} + 2I_{iy}I_{jx}) \cos 2\omega_0 t \\ & \qquad +(2I_{iy}I_{jy} - 2I_{ix}I_{jx}) \sin 2\omega_0 t \end{aligned} \tag{11.4}$$

These two tensors generated in the dephasing process possess the required property for refocusing using 180° RF pulses, namely, one being negated while the other being invariant.[1] Just as for transverse magnetisation, the phase shifts experienced by the double-quantum state may be refocused using 180° RF pulses, exactly as needed for echo formation and, more importantly, allowing phase offsets to result from the translational motion of spins in the presence of a magnetic field gradient.

Of course, the double-quantum state, having acquired the phase shifts imprinted by the spin motion, must be subsequently reconverted back to single-quantum coherence for Faraday detection. This is achieved by means of a final 90° mixing pulse, as shown in Fig. 11.1.

The doubled phase shifts experienced by the two-quantum state in a spin-echo experiment are a direct consequence of the factor of 2, on the right of eqn 11.3, effectively doubling the apparent gradient strength, or the apparent magnetogyric ratio. Later, when we come to discuss the effects of heteronuclear j-couplings, we will see that the latter perspective is the right one. In general, for an n-quantum coherence, the effective γ is multiplied by n, for example, leading, in the case of simple diffusion in a two-pulse PGSE NMR experiment, to a modified Stejskal–Tanner equation,

$$E(g) = -\exp\left(-(n\gamma g)^2 \delta^2 D(\Delta - \delta/3)\right) \tag{11.5}$$

The phase cycle

The density matrix transformations outlined all depend on perfect RF pulses. In practise RF inhomogeneity means that many spins will experience pulses that deviate from 90° or 180°, thus causing a mixing of unwanted coherences into the evolution pathway. The means by which such effects may be eliminated is outlined in Section 4.6.4. By choice of an appropriate phase cycle for the RF pulses, only desired coherences are retained. Crucial in the two-quantum PGSE experiment is that phase shifts generated under the influence of the magnetic field gradient pulses arise from evolution of a 2-QC state, with no contribution from single (or indeed any $n \neq 2$ quantum coherences), for if such unwanted states did contribute, the status of the factor n^2 in eqn 11.5 would be ambiguous. The change, Δp, in quantum order under the refocusing (third) RF pulse in Fig. 11.1(a) gives us the means by which to make our selection.

[1] In the standard spin echo, transverse magnetisation $I_x \cos\phi + I_y \sin\phi$ has one term negated and one invariant, whether a 180°_x or 180°_y RF pulse is used.

As can be seen from eqn 11.4,[2] this 180° RF pulse turns $T_{2\pm2}(11)$ into $T_{2\mp2}(11)$, and so $\Delta p = 4$. Consider then an eight-step phase cycle in which the first, second, and fourth RF pulse phases remain fixed, while the phase ϕ_3 of the third pulse is incremented in 45° steps as $\phi_3 = 0°, 45°, 90°, 135°\ldots$ From eqn 4.102 we can see that the introduced phase factor $\exp(i4\phi_3)$ will cause the final signal to alternate in sign as $1, -1, 1 - 1\ldots$ All other coherence orders will cause a quite different pattern of shifts in their contribution to the final signal. Hence by toggling the acquisition phase between 0° and 180°, and summing the successive phase cycle contributions, unwanted signals decohere and cancel as we select signal arising purely from the double-quantum coherence pathway.

The eight-step cycle can be further improved by adding a second eight steps in which the phase of the first two pulses are changed from $\phi_1 = \phi_2 = 0$ to $\phi_1 = \phi_2 = 180°$. Such a 16-step procedure has been termed a 'hexadecacycle' [10]. All phase cycles depend on such an analysis of the effects of each RF pulse. Having established the basic principles with this simple example, further unravelling of the mechanics of such phase cycles will be left as an exercise for the reader.

Gradient selection of quantum order

In Fig. 11.1(b) a different approach to the selection of desired quantum order is shown. Here a small homospoil gradient pulse of wavevector $\mathbf{q}$ is inserted into the second period during which the desired n quantum state evolves, so that $T_{2\pm2}$ evolves to $T_{2\pm2}\ \overline{\exp(\pm i2\mathbf{q}\cdot\mathbf{r})}$. Once converted back to single-quantum coherence by RF pulse 4, any refocusing of this phase-spread will occur at only the single-quantum rate, and so require twice as many homospoil pulses to generate a non-zero signal. Similarly, for selection of n-quantum coherence during the echo periods T, n homospoil pulses are needed after RF pulse 4. This method has been very effectively used by Zax and Pines to select quantum orders from 1 to 6 in a diffusion measurement on benzene dissolved in a liquid crystal, where multiple spin dipolar couplings permit higher-order coherences to be generated.

11.1.2 Use of the quadrupole interaction

Quadrupolar nuclei ($I > 1/2$) provide another opportunity for the generation of multiple-quantum states and an enhanced sensitivity to magnetic field gradients. Given that all stable quadrupolar nuclei have a magnetogyric ratio somewhat smaller that the proton, this opportunity is worth using. With quadrupolar nuclei, it is really helpful to will look at the evolution process using the spherical tensor formalism introduced in Chapter 3. Using Table 3.6, we may write, in the case of a uniaxial quadrupolar interaction, the rotating frame Hamiltonian under resonance offset $\Delta\omega$ as

$$\begin{aligned}\mathcal{H} &= \mathcal{H}_{Zeeman} + \mathcal{H}_{Q_0} \\ &= \Delta\omega T_{10} + PT_{20}\end{aligned} \tag{11.6}$$

[2] *i.e.* $T_{2\pm2}(11) = \pm(I_{ix}I_{jy} + I_{iy}I_{jx}) - i(I_{iy}I_{jy} - I_{ix}I_{jx})$ and a 180° RF pulse inverts the first term only.

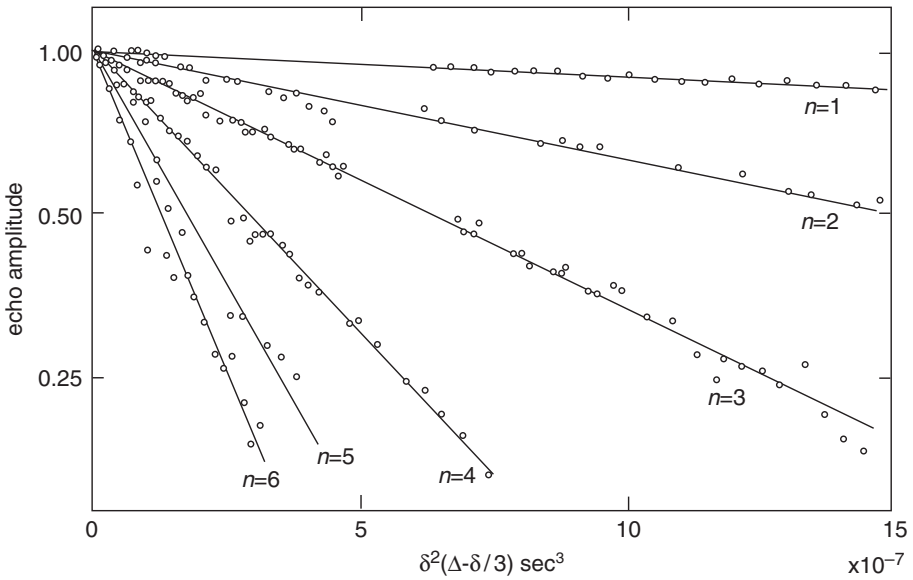

Fig. 11.2 NMR diffusion experiment for all n-quantum orders of benzene dissolved at 25% concentration in Eastman liquid crystal No. 15320. The plots show the normalised echo amplitude vs the gradient pulse timing parameters. The straight lines are linear least-squares fits to the accumulated data the slopes of which vary as n^2, indicating the increasing sensitivity to diffusion as the multiple-quantum order is increased. (Adapted from Zax and Pines [9].)

where only the secular part, $\mathcal{H}_{Q_0}$, of $\mathcal{H}_Q$ is retained, as a first-order perturbation with respect to the dominant laboratory-frame Zeeman term. P represents the strength of the quadrupolar term, and is given by

$$P = \frac{3eV_{zz}Q}{4I(2I-1)\hbar}\sqrt{6}P_2(\cos\theta) \tag{11.7}$$

where θ is the angle between the principal axis of the electric field gradient and the polarising magnetic field. For a system in which the molecule bearing the quadrupolar nuclear fluctuates rapidly between different local electric field gradient directions, but with average polar angle α, for example where the bond directions fluctuate during tumbling motion, $P_2(\cos\theta)$ may be replaced by the product of an order parameter and $P_2(\cos\alpha)$, as discussed in Section 4.4.4.

The quadrupole frequency

Suppose the spin system is excited with a 90° RF pulse to generate the density-matrix state $I_y = iT_{11}(s)$, corresponding to transverse magnetisation.[3] How will this evolve under the quadrupole interaction? For simplicity, let us start with the case $I = 1$. Figure 3.11(a) shows the relevant precession diagram, while Table 3.7 gives the

[3]Note that $T_{11}(s) = \frac{1}{\sqrt{2}}[T_{11} + T_{1-1}]$.

commutator algebra on which it is based. From the latter, it may easily be shown that, on resonance,

$$T_{11}(s) \quad \xrightarrow{PT_{20}} \quad T_{11}(s)\cos(\omega_Q t) + i(T_{21} - T_{2-1})\sin(\omega_Q t) \tag{11.8}$$

where $\omega_Q = \sqrt{\frac{3}{2}}P$. The second term in the evolved state is unobservable by Faraday detection. Hence the observable, I_y, is modulated by $\cos(\omega_Q t)$, corresponding to spectral contributions at $\pm\omega_Q$. In consequence a doublet is observed with splitting $2\omega_Q$. On this basis we could replace P in eqn 11.6 by $2\omega_Q/\sqrt{6}$.

For $I = 1$, evolution of I_y under the quadrupole interaction generated a state involving a superposition of $T_{2\pm1}$. But for higher-spin quantum numbers, while the quadrupole beat frequency remains the same, the density matrix evolution is more complex, with tensor states up to rank $k = 2I$ being generated [11]. The amplitude of these maximum rank states, $A^{1,2I}(\omega_Q t)$ are given in reference [11], up to $I = 5/2$. Under the quadrupolar interaction T_{20}, these higher-rank states, with correspondingly higher orders, q, will precess at multiples of ω_Q, so that for a spin quantum number I there are $2I$ spectral terms centred on the resonant frequency, all separated by $2\omega_Q$.

Order of quantum coherence

To understand the effect of any subsequent RF pulse, we need to return to eqn 3.65. Hard RF pulses result in simple rotations. A pulse of flip angle θ and phase ϕ with respect to the y-axis of the rotating frame transforms a spherical tensor as

$$T_{kq}(s) \quad \xrightarrow{(\theta)_\phi} \quad \sum_{q'=-k}^{k} d^{(k)}_{qq'}(\cos\theta) T_{kq'} \exp(-i\Delta q\phi) \tag{11.9}$$

$d^{(k)}_{qq'}(\cos\theta)$ being an element of the Wigner rotation matrix, and $\Delta q = q' - q$. Hence the rotation induced by an RF pulse can change the order, but not the rank, of the tensor. However, the orders generated range up to the value of the rank, each one a p-quantum coherence with p given by the q' value for that term. In the same manner that the simple two-spin dipolar interaction was used to generate double-quantum coherence, the combination of evolution under the quadrupole interaction followed by a subsequent RF pulse can generate states of multiple quantum coherence ranging up to $2I$. And of course, in accordance with eqn 3.71, such a state of coherence will precess under the Zeeman interaction of a magnetic field gradient pulse at a rate $2I$ times faster than for simple magnetisation.

The pulse sequences used to generate multiple-quantum coherence in quadrupolar systems are the same as those shown in Fig. 11.1 for the dipolar interaction. Van Dam *et al.* [12] have analysed the transfer efficiency to various coherence orders for the case where the evolution time τ following the first RF pulse is set to $\omega_Q\tau = \pi/2$. Using the relevant Wigner rotation matrix elements, they calculate the transfer efficiencies, $A^{1,2I}(\omega_Q t)$, and $A^{2I,1}(\omega_Q t)$, to generate the maximum rank states, and to return, following the final mixing pulse to transverse magnetisation, and find, for $I = 1, \frac{3}{2}, 2, \frac{5}{2}, 3$, and $\frac{7}{2}$, efficiencies of 1, $\frac{9}{10}$, $\frac{4}{5}$, $\frac{5}{7}$, $\frac{9}{14}$, and $\frac{7}{12}$.

Example for $I = \frac{3}{2}$

Van Dam *et al.* demonstrated the measurement of diffusion using a three-quantum coherence in a spin-$\frac{3}{2}$ system. Their sample comprised macroscopically ordered fibres of DNA in which lithium ions diffused. The single-quantum single-pulse spectrum of this system gives rise to a ^{7}Li quadrupolar spectrum consisting of three peaks with a quadrupolar line-splitting of 105 Hz. Figure 11.3 compares the result of a single-

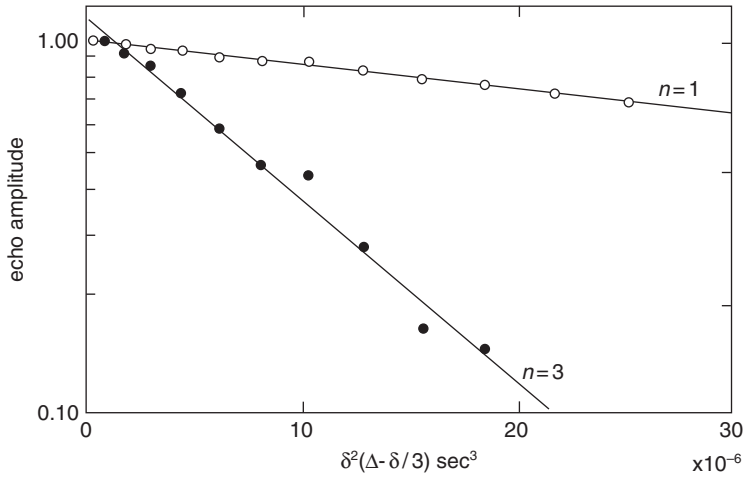

Fig. 11.3 NMR diffusion experiment for all $n = 1$- and $n = 3$-quantum states for ^{7}Li ions diffusing in a sample comprising oriented DNA fibres. The straight lines are linear least-squares fits to the data. (Adapted from van Dam *et al.* [12].)

quantum PGSE NMR experiment (open circles) with that obtained using the maximum available quantum coherence, $n = 3$ (closed circles), an experiment they refer to as total quantum PGSE or TQPGSE. Using the same diffusion coefficient for both experiments, a ratio of 2.7 is found between the square root of the slopes, close to the theoretical ratio of 3.

11.1.3 Scalar couplings and heteronuclear states

The limitations of both dipolar and quadrupole coupling approaches to the generation of multiple-quantum states are obvious. Many nuclei of interest are spin-$\frac{1}{2}$, ruling out the quadrupole route, and many systems of interest have no orientational order, making them unamenable to both quadrupolar and dipolar pathways. However, the the remaining Hamiltonian term that is also bilinear in the spin operator is the scalar coupling $2\pi J\mathbf{I}_i \cdot \mathbf{I}_j$. This interaction, which is effective in most molecules of more than rudimentary structure (the latter, sadly, including water), provides possible routes to quantum coherences and, because it acts in both heteronuclear and homonuclear mode, and like the dipolar interaction permits the formation of zero-quantum states, offers a

greater range of possibilities. One might imagine that zero-quantum coherence would be unlikely to offer amplification of the effective precession rate under the influence of a gradient pulse. However, as we shall see, in heteronuclear mode, such a gain is indeed possible.

Homonuclei

For the weak-coupling case, we may use the secular form, $2\pi J I_{iz} I_{jz}$, of the two-spin homonuclear scalar coupling and our analysis precisely mirrors the discussion in Section 11.1.1. However, greater coupling complexity exists in the case of intramolecular J-couplings, a nice example being the AMX spin system of ^{19}F nuclei in the molecule 1,1,3-trichloro-2,2,3-trifluorocyclobutane, as studied by Kay and Prestegard [13]. In this system the geminal pair has a large splitting of 200 Hz, while a weaker coupling exists between the geminal and vicinal ^{19}F.

When homonuclear couplings are used to generate two-quantum coherence, the variant of the multi-quantum PGSE sequence shown in Fig. 11.1(b) is desirable, the 180° RF pulses in the evolution period (along with that in the multiquantum echo) acting to refocus heteronuclear couplings and chemical shifts. For the molecule used in reference [13], and given suitable phase cycling, the two J-couplings lead, at the end of the preparation period τ, to a double-quantum state with amplitudes determined by J_{12} as well as J_{13}, and J_{23}, i.e.

$$\rho_{2QT} = (2I_{ix}I_{2y} + 2I_{1y}I_{2x}) \cos(\pi J_{12}\tau) \left(\cos(\pi J_{13}\tau) + \cos(\pi J_{23}\tau)\right) \tag{11.10}$$

where $i = 1, 2$ refers to the geminal fluorines, while $i = 3$ refers to the vicinal ^{19}F in this molecule. Given $J_{12} \gg J_{13}, J_{23}$, maximum amplitude is achieved for $\tau = 1/2J_{12}$, leading to a double-quantum state with amplitude $(\cos(\pi J_{13}/2J_{12}) + \cos(\pi J_{23}/2J_{12}))$. Such subtle modulation effects will generally be a feature of multiple-quantum coherence generated by homonuclear couplings, each molecule requiring its own density matrix evolution analysis.

Heteronuclei

With heteronuclear couplings used to generate multi-quantum states, an interesting questions arises. Just what is the multiplication factor for γ given that more than one magnetogyric ratio plays a role? This question was first addressed by Kuchel and Chapman [14], who demonstrated measurement of diffusion under double-quantum coherence in the heteronuclear coupled system ^{1}H-^{31}P in neutralised phosphoric acid, and later by Dingley *et al.* [15] for both double and zero-quantum coherence using the ^{1}H-^{15}N coupling for a protein in aqueous solution.

Suppose we consider a state of two-quantum coherence generated between a nucleus I and a heteronucleus S, namely $I_xS_y + I_yS_x$, and allow each nucleus to to evolve under its imposed Zeeman interactions, $\gamma_I B I_z$, and $\gamma_S B S_z$, to be acted on by 180° RF pulses for each nucleus, and to evolve under a differing Zeeman field B', such as might result from the fields resulting from applied gradient, with intervening translational motion. We could write

$$
\begin{aligned}
& I_xS_y + I_yS_x \\
& \xrightarrow{-(\gamma_I B I_z + \gamma_S B S_z)} \quad (I_x\cos\phi_I - I_y\sin\phi_I)(S_y\cos\phi_S + S_x\sin\phi_S) \\
& \qquad\qquad +(I_y\cos\phi_I + I_x\sin\phi_I)(S_x\cos\phi_S - S_y\sin\phi_S) \\
& \xrightarrow{-(\pi/2)(I_y+S_y)} \quad (-I_x\cos\phi_I - I_y\sin\phi_I)(S_y\cos\phi_S - S_x\sin\phi_S) \\
& \qquad\qquad +(I_y\cos\phi_I - I_x\sin\phi_I)(-S_x\cos\phi_S - S_y\sin\phi_S) \\
& \xrightarrow{-(\gamma_I B' I_z + \gamma_S B' S_z)} \quad (-I_x(\cos\phi_I\cos\phi'_I + \sin\phi_I\sin\phi'_I) \\
& \qquad\qquad -I_y(\sin\phi_I\cos\phi'_I - \cos\phi_I\sin\phi'_I)) \\
& \qquad\qquad \times(S_y(\cos\phi_S\cos\phi'_S + \sin\phi_S\sin\phi_S) \\
& \qquad\qquad -S_x(\sin\phi_S\cos\phi'_S - \cos\phi_S\sin\phi'_S)) \\
& \qquad\qquad +(I_y(\cos\phi_I\cos\phi'_I + \sin\phi_I\sin\phi'_I) \\
& \qquad\qquad -I_x(\sin\phi_I\cos\phi'_I - \cos\phi_I\sin\phi'_I)) \\
& \qquad\qquad \times(-S_x(\cos\phi_S\cos\phi'_S + \sin\phi_S\sin\phi_S) \\
& \qquad\qquad -S_y(\sin\phi_S\cos\phi'_S - \cos\phi_S\sin\phi'_S)) \\
& = \qquad\qquad -(I_xS_y + I_yS_x)\cos(\Delta\phi_I + \Delta\phi_S) \\
& \qquad\qquad +(I_xS_x - I_yS_y)\sin(\Delta\phi_I + \Delta\phi_S) \qquad (11.11)
\end{aligned}
$$

where $\Delta\phi_I + \Delta\phi_S = \phi_I - \phi'_I + \phi_S - \phi'_S$. We see that the state of double-quantum coherence precesses at a rate given by the sum of the I and S spin Larmor frequencies, and that in the PGSE experiment the phase offset due to translational motion is the sum of that experienced by the I and S spins. It is as though the effective magnetogyric ratio of the heteronuclear double-quantum coherence state is $\gamma_S + \gamma_I$.

As an exercise, the reader could follow the same process for the heteronuclear zero-quantum coherence state $I_xS_y - I_yS_x$. Now we find that the effective magnetogyric ratio is $\gamma_S - \gamma_I$. By the way, there is no doubt that for heteronuclear scalar couplings, product operator algebra is more transparent than is possible using spherical tensors

The pulse sequence used by Kuchel and Chapman is shown in Fig. 11.4(a). It is based on the inverse DEPT sequence [16].[4] The experiment starts with an excitation of the heteronucleus, ^{31}P, labelled S, but with final detection on the more sensitive proton, here labelled I. In this example, a simple two-spin heteronuclear coupling, $2\pi JI_zS_z$, applies. Because of the markedly different Larmor frequencies in the heteronuclear case, this secular approximation is effectively exact. It is instructive to follow the density matrix through the time points, shown in Fig. 11.4(a), using the initial step of the phase cycle [14], $\phi_1 = x$, $\phi_2 = x$, $\phi_3 = y$, $\phi_4 = x$, $\phi_5 = x$, $\phi_6 = x$, $\phi_7 = -y$, acquisition phase $= y$. These states are as follows:

$$
\begin{aligned}
\rho_1 &= I_z + S_z \\
\rho_2 &= I_z + S_y \\
\rho_3 &= I_z + S_y\cos(\pi J\tau_1) - 2I_zS_x\sin(\pi J\tau_1) \\
\rho_4 &= I_y - S_y\cos(\pi J\tau_1) - 2I_yS_x\sin(\pi J\tau_1) \qquad (11.12)
\end{aligned}
$$

[4]Also known as heteronuclear multiple-quantum coherence (HMQC).

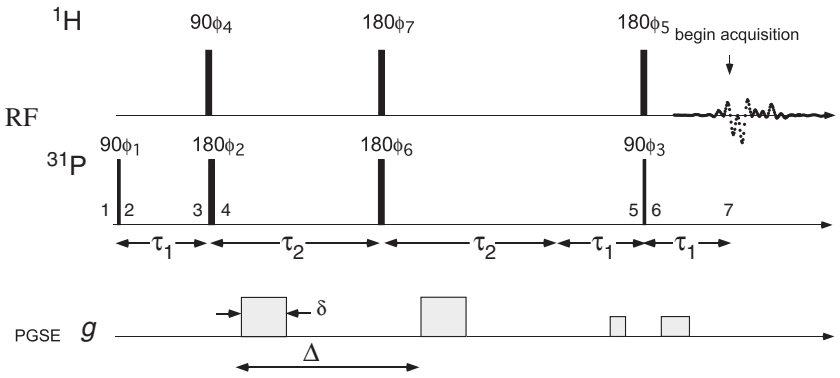

Fig. 11.4 Pulse sequence based on inverse DEPT used to measure diffusion via the double-quantum state generated by the heteronuclear ^{31}P-^{1}H J coupling. The phase labels follow those used in reference [14], and specific evolution points of the density matrix are marked with numerals. Note the selection of coherence order by careful choice of homospoil pulses. (Adapted from Kuchel and Chapman [14].)

By the choice $\tau_1 = 1/2J$, or any odd multiple of $1/2J$, a partial state of two-quantum coherence is generated,[5] so that $\rho_4 = I_y - 2I_yS_x$. The subsequent PGSE echo over the time period $2\tau_1$, involving 180° RF pulses for both I and S spins, serves to refocus any chemical shift dephasing over that period. Meanwhile the J coupling acts relentlessly on I_y over the total time period, while, of course, the two-quantum coherence state, I_yS_x is invariant under the scalar coupling. Neglecting for the moment the Zeeman precession under the PGSE gradient pulses, this brings us to density matrix state 5 where

$$\begin{aligned}
\rho_5 &= I_y \cos(\pi J(2\tau_2 + \tau_1)) - 2I_xS_z \sin(\pi J(2\tau_2 + \tau_1)) - 2I_yS_x \\
\rho_6 &= -I_y \cos(\pi J(2\tau_2 + \tau_1)) + 2I_xS_x \sin(\pi J(2\tau_2 + \tau_1)) + 2I_yS_z \\
\rho_7 &= \text{“}\textit{unobservables}\text{”} - I_x,
\end{aligned} \tag{11.13}$$

The first term in ρ_6 is rendered unobservable by the unequal area homospoil pulses which sandwich the final RF pulse. The second term clearly remains unobservable while the final I_yS_z term precisely evolves to the observable $-I_x$ over the duration τ_1.

Note that the density matrix term I_yS_x existing over the PGSE echo period is only part of the full two-quantum coherence state. The remaining I_xS_y component could be generated in the latter steps of a phase cycle, but this is unnecessary. We can instead regard I_xS_y as a superposition of the double quantum state $I_xS_y + I_yS_x$ and the single quantum state $I_xS_y - I_yS_x$, and then ensure that remaining parts of the pulse sequence select for the former. The means by which this is achieved is via the use of a pair of homospoil gradient pulses before and after the final RF pulses. This results in precession of the $2I_yS_x + 2I_xS_y$ component, from which the final observable derives,

[5] I_yS_x is a superposition of double- and zero-quantum coherence.

at rate given by an effective magnetogyric ratio, $\gamma_S + \gamma_I$, while the zero quantum part, $2I_yS_x - 2I_xS_y$ precesses at a rate determined by $\gamma_S - \gamma_I$. After the last RF pulse, the observable term precesses at γ_I. Thus for double quantum coherence selection, the ratio of the pulse areas before and after the last RF pulse needs to be $\gamma_I/(\gamma_S + \gamma_I)$.

Now we see the answer to our question. During the multiple-quantum coherence, and compared with a single-quantum PGSE experiment using spin I, the precession rate is enhanced, not by n^2 as in eqn 11.5, but by [14]

$$n^2 \rightarrow \left(\frac{\gamma_s + \gamma_I}{\gamma_I}\right)^2 \tag{11.14}$$

Equation 11.14 poses an interesting problem. Suppose γ_s and γ_I have opposite sign? In that case we will be worse off by travelling via the double-quantum pathway. The solution, proposed by Dingley *et al.*, is to employ the state of zero-quantum coherence, where $\gamma_S - \gamma_I$ is the effective magnetogyric ratio. This opposite sign situation applies in ^{1}H-^{15}N experiments, highly relevant for isotopically labelled proteins.[6]

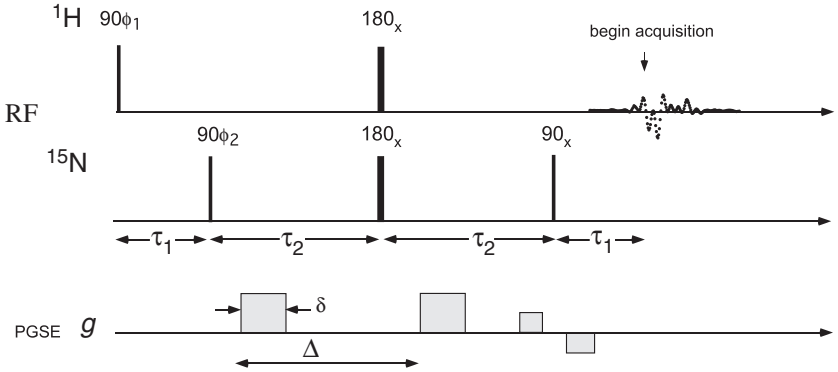

Fig. 11.5 Modified version of Fig. 11.4. (Adapted from Dingley *et al.* [15].) Note again the selection of coherence order by careful choice of homospoil pulses.

Their pulse sequence, shown in Fig. 11.5, is a simplified version of that used by Kuchel and Chapman, which also generates a mixture of double- and zero-quantum coherence. Using the methods outlined above, it is a straightforward process to derive the density matrix at various steps of the evolution pathway. The important point to note is that the final homospoil gradient selection filter is designed to select the zero-quantum state from the PGSE evolution period.

Remarks on multiple-quantum PGSE NMR

In the discussion so far, no reference has been made to that bugbear of PGSE NMR, the loss of signal due to transverse relaxation while the spin ensembles are being encoded for translational motion. In most of the examples discussed, where relaxation

[6] $\gamma_{^1H} = 267.513$ rad s^{-1} T^{-1} and $\gamma_{^{15}N}$ =-27.116 rad s^{-1} T^{-1}.

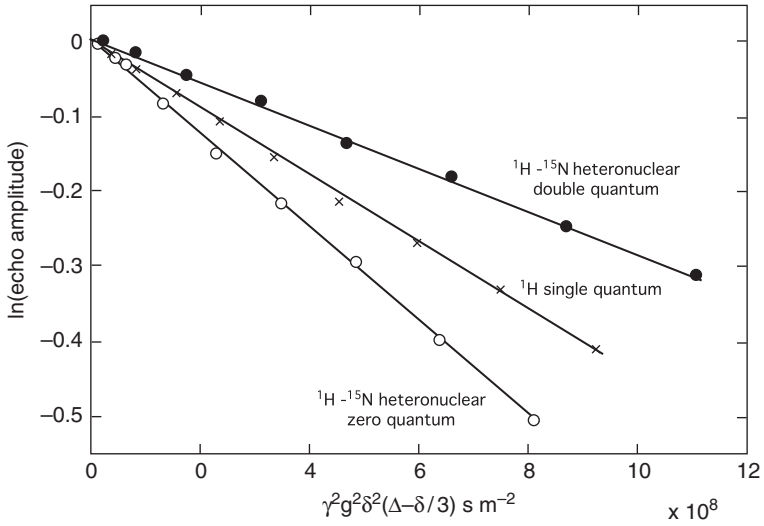

Fig. 11.6 Showing the sensitivity of different coherence orders to field-gradient pulses for ^{1}H-^{15}N heteronuclear states in selected ubiquitin resonances. Paradoxically, the zero-quantum coherence is most sensitive to diffusion because of the opposite signs of the ^{1}H and ^{15}N magnetogyric ratios. The ratios of the slopes obtained from these fits are 0.65 and 1.36 for DQ/SQ and ZQ/SQ, respectively, which are in reasonable agreement with the theoretical values of 0.81 and 1.21 (see eqn 11.14). (Adapted from Dingley *et al.* [15].)

rates are quoted, these are not significantly worse in double-quantum states, perhaps up to a factor of two, and in some cases longer [8]. However, the generation of these higher-order quantum states does require additional evolution time in the transverse plane and hence greater T_2 relaxation loss.

Before leaving this topic, it is worth remarking that uses of multiple-quantum coherence to measure diffusion, despite increase sensitivity in the precession, are, in addition to those discussed above, remarkably few [17, 18], probably reflecting the greater complexity of the pulse sequences needed, as well as the loss of signal due to additional relaxation and inefficiency in coherence transfer and selection.

11.2 Singlet states and time extension

One factor that limits PGSE NMR is the upper limit to available time window, Δ, for molecular migration, T_2 and the longer T_1 for spin and stimulated echoes respectively. For most liquids, T_1 values range from 100 ms for macromolecules in solution to around 10 s in de-oxygenated water. In nearly every case, T_1 relaxation arises from dipolar interactions, primarily intramolecular, since the internuclear proximity r affects the relaxation rate as r^{-6}, though more distant intermolecular dipolar interactions will also contribute. In what follows we see how to suppress the effect of intramolecular dipole–dipole interactions, given suitable conditions, and how this suppression can

lend itself to the production of nuclear spin coherences sufficiently long-lived to allow much longer molecular migration times, Δ.

11.2.1 Product states, singlet–triplet states, and symmetry

Consider a pair of nuclear spins with scalar coupling J and chemical shift difference $\Delta\omega$. Let us assume they are homonuclei, calling them I_1 and I_2. Provided the chemical shift difference is much larger than the coupling, i.e. $\Delta\omega \gg 2\pi J\hbar$, then the product operator basis $\{|\uparrow\uparrow\rangle, |\uparrow\downarrow\rangle, |\downarrow\uparrow\rangle, |\downarrow\downarrow\rangle\}$ is approximately diagonal,[7] and the scalar coupling may be treated as a first-order perturbation, $2\pi J I_{1z} I_{2z}$. If on the other hand $\Delta\omega \ll 2\pi J\hbar$, the near-diagonal basis is the singlet–triplet set $\{|S_0\rangle, |T_{-1}\rangle, |T_0\rangle, |T_1\rangle\}$ where

$$\begin{aligned} |S_0\rangle &= \sqrt{\tfrac{1}{2}}\,[|\uparrow\downarrow\rangle - |\downarrow\uparrow\rangle] \\ |T_{-1}\rangle &= |\uparrow\uparrow\rangle \\ |T_0\rangle &= \sqrt{\tfrac{1}{2}}\,[|\uparrow\downarrow\rangle + |\downarrow\uparrow\rangle] \\ |T_1\rangle &= |\downarrow\downarrow\rangle \end{aligned} \tag{11.15}$$

and the full scalar coupling $2\pi J\mathbf{I_1}\cdot\mathbf{I_2}$ is diagonal, with the good quantum numbers provided by the total angular momentum I, and its azimuthal projection m. $I = 0$ and $m = 0$ for the singlet and $I = 1$ and $m = 1, 0, -1$ for the triplet. Note that the singlet state is antisymmetric under exchange of spins 1 and 2, while the triplet states are symmetric. Further details concerning operator algebra for the product and singlet–triplet bases, and transformations between these bases can be found in reference [19].

Now consider the through-space intramolecular dipole–dipole interaction between spins 1 and 2. As pointed out by Caravetto and Levitt [20–22], this interaction is symmetric under exchange of the spins and therefore cannot couple singlet and triplet states. As a result, a non-equilibrium state containing a population difference between the singlet and triplet manifolds cannot be brought into equilibrium by intramolecular dipole–dipole relaxation alone, while relaxation between the various sub-manifolds of the triplet state is indeed possible, and is indeed the basis of T_1 relaxation for the two-spin system. When the chemical shift $\Delta\omega$ is non-zero, the singlet and triplet states are admixed, so that T_1 relaxation applies to the whole spin system. If $\Delta\omega = 0$ then the singlet state may be isolated, and its T_1 relaxation suppressed. What will remain will be a much slower relaxation process, T_S, perhaps involving the much weaker dipolar interactions from more distant spins.

Why then do we not normally see this slower relaxing component in coupled spin systems? First, the thermal equilibrium density matrix state, $I_{1z} + I_{2z}$, is a superposition of T_1 and T_{-1} with no S_0 component. Even if we could transfer coherence to S_0, the singlet state generates no net magnetisation and cannot be observed directly in a conventional NMR experiment.

[7] Some authors use α to represent spin-up ($\frac{1}{2}$) and β for spin-down ($-\frac{1}{2}$).

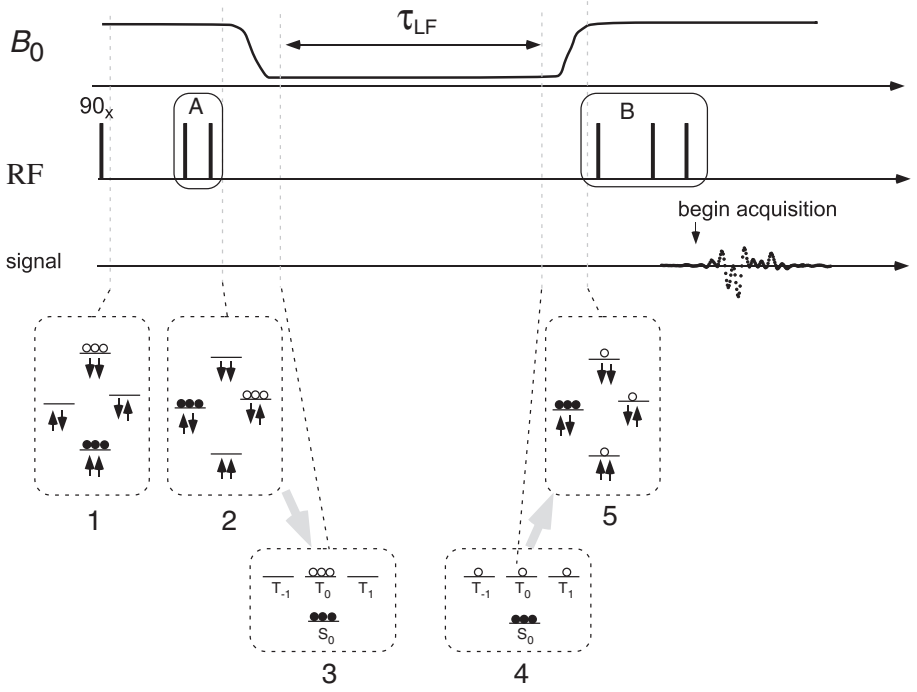

Fig. 11.7 Schematic idea of transfer of magnetisation to singlet state for-long term storage over time τ_{LF}, during which relaxation occurs at a rate T_S^{-1}, much slower than T_1^{-1}. In this version, the singlet state is isolated from the triplet by reducing the magnetic field strength. A suitable RF pulse train can achieve the same effect. Pulse segment A performs conversions from magnetisation states $I_{1x} + I_{2x}$ and $2I_{1x}I_{2z} + 2I_{1z}I_{2x}$ to the superposition of singlet and triplet states, while B returns the coherence to detectable magnetisation, $I_{1x}+I_{2x}$ or $I_{1y}+I_{2y}$. During τ_{LF}, relaxation occurs amongst the triplet sub-levels while the singlet is protected. (Adapted from Carravetta *et al.* [20].)

Levitt and co-workers discuss the potential for coherence transfer in and out of the singlet state. In systems where the coupled spins are in equivalent chemical sites ($\Delta\omega = 0$), there is no obvious mechanism to convert $I_{1z} + I_{2z}$ to the long-lived singlet state by population transfer to or from other spin states, since most experimental manipulations such as RF pulses, or evolution under to the spin Hamiltonian, act symmetrically on the two spins [22]. And so we turn our attention back to to systems where the coupled spins are in non-equivalent chemical sites ($\Delta\omega \neq 0$). Here the manipulation tools are available, but once the transfer to the singlet state has taken place, the chemical shift interaction breaks the spin exchange symmetry, thereby destroying any dynamic isolation.

The trick then is to be able to turn the chemical shift on and off at will. As Levitt *et al.* point out, this can be done by lowering the polarising field B_0 or by the use of refocusing the RF pulse train. The latter is clearly the easier route! Therein lies the potential for creating a slowly relaxing state.

11.2.2 Sequence for translation measurement

The first demonstration of diffusion measurement using a long-lived singlet state was by Bodenhausen, Cavadini, and co-workers [23], using the simple scalar two-spin system [21], 2-chloroacrylonitrile (i.e., $H_{I_1}H_{I_2}C{=}CRR'$ with R = Cl and R = CN. The coherence evolution pathway chosen is to first excite a zero-quantum coherence, $ZQC_y = \frac{1}{2}(2I_{1y}I_{2x} - 2I_{1y}I_{2x})$, and allow it to evolve under the effects of the chemical shifts into $ZQC_x = \frac{1}{2}(2I_{1x}I_{2x} + 2I_{1y}I_{2y})$. RF irradiation at the midpoint between the I_1 and I_2 resonances leads to the suppression of the chemical shifts, while the $2\pi J\mathbf{I_1}\cdot\mathbf{I_2}$ interaction remains, converting the two-spin system into one where the two nuclei have, in effect, become magnetically equivalent. In the process, the two eigenstates $|\uparrow\downarrow\rangle$ and $|\downarrow\uparrow\rangle$ become degenerate and can be expressed as a superposition of a triplet state $|T_0\rangle\langle T_0|$ and a singlet state $|S_0\rangle\langle S_0|$, the zero-quantum coherence ZQC_x becoming $\frac{1}{2}(|T_0\rangle\langle T_0| - |S_0\rangle\langle S_0|)$, and then, over the irradiation period T, the triplet component relaxing as T_1 and the singlet relaxing much more slowly as T_S.

Figure 11.8 shows the pulse sequence used to generate the singlet state for the purpose of diffusion measurement. For the moment we will ignore the effect of the gradient pulses and focus solely on the coherence transfers, using a rotating frame with reference frequency ω_0 centred between the two resonant frequencies, ω_1 and ω_2. After the first $90^\circ_x - \tau_1 - 180^\circ_x - \tau_1$ RF pulse sandwich, with $2\tau = 1/2J$, chemical shift offsets have been refocused and the initial longitudinal magnetisation $I_{1z} + I_{2z}$ has been converted to $-2I_{1x}I_{2z} - 2I_{1z}I_{2x}$. Suppose the next interval, τ_2, is set to the 'difference precession interval' $\pi/(2|\omega_0 - \omega_{I_1}|) = \pi/(2|\omega_0 - \omega_{I_2}|) = \pi/(|\omega_{I_1} - \omega_{I_2}|)$. Then the transverse components undergo a precession in opposite directions through one-quarter of a full cycle and at the end of τ_2 one is left with the density matrix state $2I_{1y}I_{2z} - 2I_{1z}2I_{2y}$ and the 90°_y pulse at the end of the τ_2 interval converts this into $2I_{1y}I_{2x} - 2I_{1x}2I_{2y}$, the state of zero-quantum coherence, ZQC_y.

The next interval, τ_3 is half τ_2, i.e. $\tau_3 = \pi/(2|\omega_{I_1} - \omega_{I_2}|)$, allowing ZQC_y to precess into $ZQC_x = 2I_{1x}I_{2x} + 2I_{1y}2I_{2y}$, and, at the onset of RF irradiation, when magnetic equivalence is established, ZQC_x may be rewritten $\frac{1}{2}(|T_0\rangle\langle T_0| - |S_0\rangle\langle S_0|)$. During the irradiation for period T, the triplet state relaxes at rate T_1^{-1}, leaving only $-\frac{1}{2}|S_0\rangle\langle S_0|$ surviving. When the RF is switched off at the end of the period T, the chemical shift once more breaks the symmetry and $-\frac{1}{2}|S_0\rangle\langle S_0|$ may be rewritten in the product basis as $-\frac{1}{2}(I_{1x}I_{2x} + I_{1y}I_{2y}) - I_{1z}I_{2z} + \frac{1}{2}(I_{1x}I_{2y} - I_{1y}I_{2x})$. Note that this superposition is invariant under a Zeeman Hamiltonian and is therefore unaffected by any homospoil gradient pulse. By this means, unwanted coherences may be removed by a homospoil pulse, while the desired superposition state is preserved.

As an exercise to make the process explicit for the reader, we can follow the density matrix through the time points, shown in Fig. 11.8. These states are as follows:

$$
\begin{aligned}
\rho_1 &= I_{1z} + I_{2z} \\
\rho_2 &= I_{1y} + I_{2y} \\
\rho_3 &= I_{1y}\cos(\pi J\tau_1) - 2I_{1x}I_{2z}\sin(\pi J\tau_1) + I_{2y}\cos(\pi J\tau_1) - 2I_{1z}I_{2x}\sin(\pi J\tau_1) \\
&= -2I_{1x}I_{2z} - 2I_{1z}I_{2x} \\
\rho_4 &= 2I_{1y}I_{2z} - 2I_{1z}I_{2y}
\end{aligned}
$$

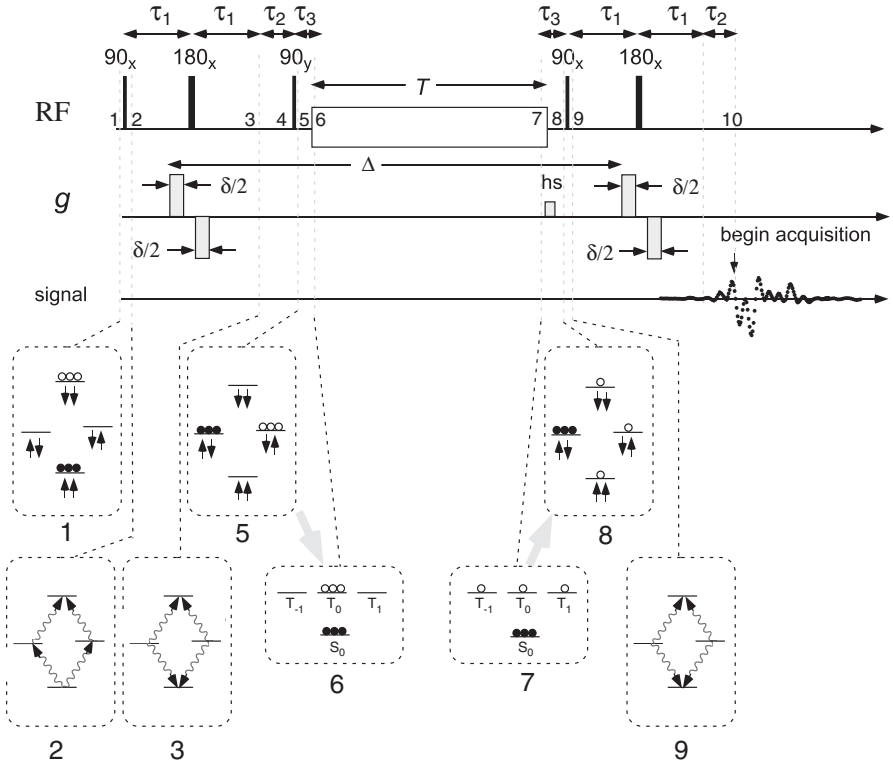

Fig. 11.8 Singlet-state single-quantum diffusion pulse sequence applicable to a molecule with a two-spin scalar coupling. The information about spatial localisation is stored in the form of singlet state populations with a relaxation time T_s during the interval T, while RF irradiation is applied at the midpoint of the Larmor frequencies of the spins. The intervals τ_1, τ_2, and τ_3 are chosen, as described in the text, to cause specific evolutions of the density matrix that generate the desired pathway. (Adapted from Cavadini *et al.* [23].)

$$\begin{aligned}\rho_5 &= 2I_{1y}I_{2x} - 2I_{1x}I_{2y}\\ \rho_5 &= 2I_{1x}I_{2x} + 2I_{1x}I_{2x}\end{aligned} \tag{11.16}$$

RF irradiation during the period T, with the transmitter set at the midpoint between the resonances at ω_1 and ω_2, and using an RF field amplitude such that the nutation frequency is well in excess of the difference $\omega_1 - \omega_2$, essentially spin-locks the density matrix in the new Zeeman frame of the RF field, where now I_1 and I_2 have a common Larmor frequency.[8] The scalar coupling, $2\pi\mathbf{I_1} \cdot \mathbf{I_2}$ is unaffected by the RF field and remains to act on the spin system, with eigenstates of the pure singlet–triplet basis. Thus the ZQC_x state of ρ_6 must be transformed to the new basis:

[8]Yes, the chemical shift still remains, but since it is proportional to the RF field amplitude rather than the B_0 field amplitude, its absolute size is insignificant compared with the unmodified scalar coupling. Hence strong coupling conditions are established.

$$\begin{aligned}
\rho_6 &= \tfrac{1}{2}(|T_0\rangle\langle T_0| - |S_0\rangle\langle S_0|) \\
\rho_7 &= -\tfrac{1}{2}|S_0\rangle\langle S_0| \\
\rho_7 &= -\tfrac{1}{2}(I_{1x}I_{2x} + I_{1y}I_{2y}) - I_{1z}I_{2z} + \tfrac{1}{2}(I_{1x}I_{2y} - I_{1y}I_{2x}) \\
\rho_8 &= \tfrac{1}{2}(I_{1y}I_{2y} - I_{1x}I_{2x}) - I_{1z}I_{2z} + \tfrac{1}{2}(I_{1y}I_{2x} - I_{1x}I_{2y}) \\
\rho_9 &= -\tfrac{1}{2}(I_{1z}I_{2z} + I_{1x}I_{2x}) - I_{1y}I_{2y} - \tfrac{1}{2}(I_{1x}I_{2z} + I_{1z}I_{2x})
\end{aligned} \tag{11.17}$$

With no more RF pulses to follow, only the last term of ρ_9 can contribute to observable magnetisation and so

$$\begin{aligned}
\rho_9 &= -\tfrac{1}{2}(I_{1x}I_{2z} + I_{1z}I_{2x}) \\
\rho_{10} &= \tfrac{1}{2}(I_{1y} + I_{2y})
\end{aligned} \tag{11.18}$$

Finally, we consider the effect of the bipolar gradient pairs placed around the 180° RF pulses, thus giving them the same effective sign, with total pulse q-vector amplitude $\gamma g \delta$. The two pairs act to induce phase shifts $\phi = \mathbf{q} \cdot \mathbf{r}$ and $\phi' = \mathbf{q} \cdot \mathbf{r}'$, depending on the locations $\mathbf{r}$ and $\mathbf{r}'$ of the spin-bearing molecules at the respective times of encoding separated by time interval Δ. The final signal therefore is modulated by a ensemble average factor $\overline{\cos\phi\cos\phi'} = \frac{1}{2}\left(\overline{\cos(\phi - \phi')} + \overline{\cos(\phi + \phi')}\right)$, the latter term averaging to zero over the sample, while the first, $\frac{1}{2}\overline{\cos(\phi - \phi')}$, comprises the desired encoding for motion.

There many ways in which the singlet state may be generated and used for diffusion measurement. The pulse sequence of reference [23], which is analysed above, is one example. However, by understanding in detail the mechanism of one such example, the reader can easily invent other schemes [19, 24]. The crucial factor is that the process is relatively uncomplicated and easy to implement. The trick is to find the molecule with the desired dominant two-spin scalar coupling.

Finally, it is worth noting that the prerequisite for creating the singlet state, namely the existence of the intramolecular two-spin scalar coupling, also enables the generation of two-quantum coherence. By this means the enhanced diffusion sensitivity discussed in Section **??** and the enhanced diffusion timescale enabled by singlet state creation can be combined in the one experiment [23].

11.2.3 Measurement of diffusion via the singlet state

The first point to establish in a practical implementation of singlet-state time extension is the degree to which T_S exceeds T_1. In the $\mathrm{H}_{I_1}\mathrm{H}_{I_2}$C=CRR' example of Cavadini *et al.* [23], the result is really quite spectacular, as can be seen in Fig. 11.9, with well over an order of magnitude achieved.

The singlet state method has been used effectively to measure the diffusion of the 2-chloroacrylonitrile at diffusive observation times of up to 20 s, an example of such a measurement obtained at $\Delta = 12$ s being shown in Fig. 11.10. Even with the loss of $\frac{1}{2}$ signal amplitude during the storage of the singlet state, the time extension available with decay at the rate T_S^{-1}offers a very significant advantage over traditional z-storage, where T_1 relaxation would normally result in a severe loss of signal amplitude over a storage period of a few seconds.

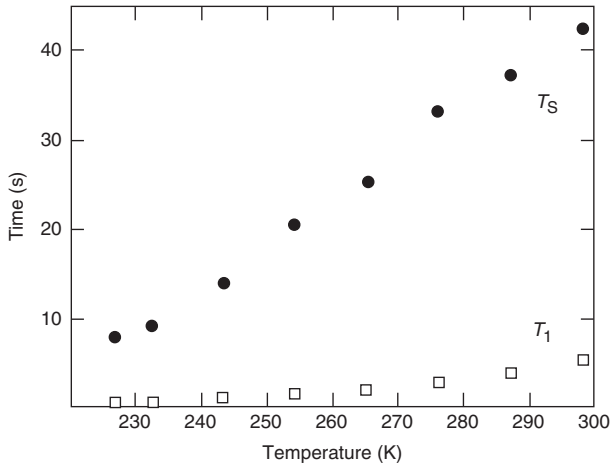

Fig. 11.9 Temperature dependence in the range from –46 to +25°C (227 to 298 K) of the spin-lattice relaxation time T_1 and the singlet state lifetime T_S of the protons I_1 and I_2 in 10 mM 2-chloroacrylonitrile, $H_{I_1}H_{I_2}C{=}CClCN$, dissolved in a mixture of deuterated DMSO-d6/D_2O. (Adapted from Cavadini *et al.* [23].)

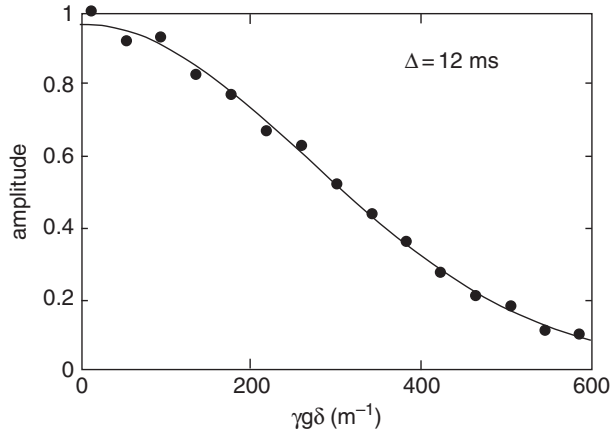

Fig. 11.10 Echo amplitude versus q-vector amplitude from the protons I_1 and I_2 in the 10 mM 2-chloroacrylonitrile $H_{I_1}H_{I_2}C{=}CClCN$/deuterated DMSO-d6/D_2O system of reference [23] obtained at 245 K and with diffusion observation time Δ=12 ms. The Gaussian decay is fitted using the Stejskal–Tanner relation to yield a diffusion coefficient of $(5.7 \pm 0.2) \times 10^{-11}$ m^{2}s^2. (Adapted from Cavadini and Vasos [19].)

11.3 Intermolecular quantum coherence

It has long been known that in samples with large magnetisation density, non-linearities play a role in the Bloch equations, resulting in complex evolution of the spin

magnetisation. A classic example of such a phenomenon is the effect of radiation damping [25], where induced emfs in the receiver coil are sufficiently large to interact back on the precessing magnetisation, thus causing a free-induction decay rate faster than that due to relaxation alone. However, in 1979 Deville *et al.* [1] discovered multiple echoes in ^{3}He NMR experiments which appeared to arise from intermolecular dipolar interactions. Even more remarkably, Warren and co-workers in 1993 demonstrated, in two-dimensional proton NMR experiments, the appearance of cross peaks between protons on molecules of completely different molecular species, indicative of intermolecular multiple-quantum transitions [3, 4]. Warren *et al.* argued that the origin of these intermolecular coherences was the same long-range dipolar field responsible for the appearance of multiple echoes following a simple two RF pulse spin-echo sequence, presenting in the process a convenient quantum description based on density matrix formalism.

The 1993 experiment [3, 4] that caused such surprise to the NMR community was dubbed by its authors 'CRAZED'[9], a suitable title given the level of consternation that resulted. A schematic example of the experiment is shown in Fig. 11.11, involving proton cross-peaks from benzene and chloroform molecules in a liquid mixture, found in a two dimensional correlation experiment in which gradient pulse filters are used to select for two-quantum coherence during the t_1 evolution period. The results astound for three specific reasons. First, there are no J-couplings that can cause magnetisation transfer between different molecular species; indeed for these molecules, there are no *intramolecular* J-couplings, because of the simple chemically equivalent nature of the hydrogens in each molecular species. Second, we are dealing with a liquid, in which rapid molecular tumbling is more than adequate at removing spin-pairwise intermolecular dipolar couplings at all length scales, a matter we shall address in more detail in Section 11.3.1. Third, we have to ask, how can there exist a state of two-quantum coherence after the first 90_x RF pulse, when no obvious bilinear spin term in the Hamiltonian is present to help create such a coherence? In any case, our experience suggests the need for at least two RF pulses sandwiching evolution under a bilinear secular term, if two-quantum coherence is to be created. CRAZED not only challenges some of our deepest assumptions but it provides a warning that we need to be alert to unexpected signals in NMR experiments in simple liquids, especially where magnetic field gradients are used. For this reason alone, these effects are of interest to experimenters carrying out PGSE NMR or NMR imaging experiments.

While the original multi-echo experiments were explained through an understanding of the role of non-linearities in the Bloch equations arising from the distant dipolar field, CRAZED, with its remarkable resemblance to quantum coherence effects, called out for fresh insight. As a consequence, a significant debate took place regarding the precise physical origin of all these experimental phenomena. While there was agreement that the additional demagnetising field arising from long-range dipolar interactions was central to any understanding of these effects, the dispute concerned whether these arose solely from classical Bloch equation non-linearities, or whether the effects were inherently quantum mechanical in origin. Thanks to a cooperative effort by several interested authors [5, 26, 27], we now understand that the effects

[9]Correlated 2-D spectroscopy Revamped by Asymmetric Z-gradient Echo Detection.

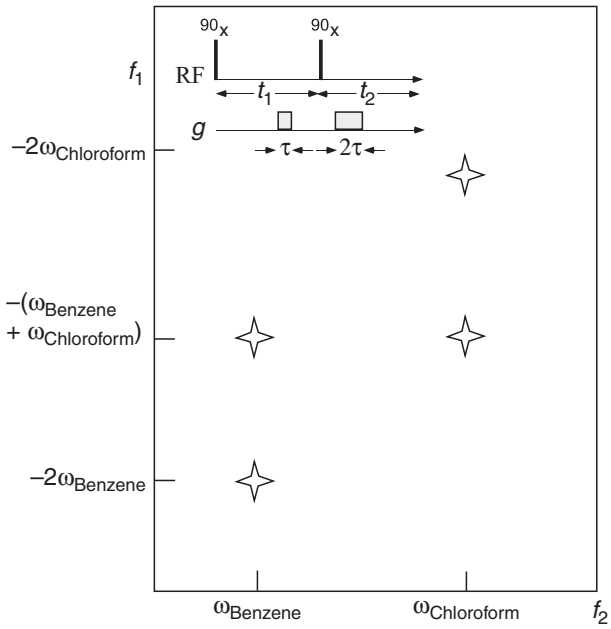

Fig. 11.11 CRAZED spectrum of a mixture of benzene and chloroform. The inset shows the simple two RF pulse sequence along with coherence-selecting homospoil gradient pulses. By conventional theory, this spectrum should be blank. Instead, there are peaks with all properties of intermolecular double-quantum peaks. (Adapted from Richter and Warren [7].)

of classical non-linearities and a description based on quantum coherence phenomena really are one and the same.

11.3.1 The quantum description

What made the quantum description of Warren *et al.* so appealing was its inherent simplicity, its connection with well-understood NMR density matrix operator algebra, and its ability to explain previously unobserved phenomena. In particular, the experimental demonstration of echo order selection by means of homospoiling gradient pulses of differing duration could be explained—exactly as is found in multiple-quantum coherence phenomena in high resolution NMR experiments in which bilinear terms in the spin Hamiltonian provide the means to explore different coherence pathways. At the heart of the physics is the existence of high-order terms in the equilibrium density matrix. Indeed, the breakdown of the usual high temperature approximation (HTA) is central to Warren's description. Furthermore the quantum operator formalism requires that we represent ensemble-averaged spin behaviour, namely the collective sum of pairwise dipolar interactions, in the same manner as we would represent a simple two-spin interaction through a single term in the spin Hamiltonian. These unusual requirements, which can be formally justified, allow for very familiar and NMR-relevant treatment of the intermolecular dipolar phenomena.

Examination of the high-temperature approximation

We start by considering the density matrix in thermal equilibrium,

$$\rho_{eq} = \frac{\exp(-\beta\mathcal{H})}{Tr\left(\exp(-\beta\mathcal{H})\right)} \tag{11.19}$$

where $\beta = 1/k_BT$. In the case of an N-spin system of coupled spin-$\frac{1}{2}$ particles, $\mathcal{H}$ is a $2N \times 2N$ matrix and is given by

$$\mathcal{H} = \sum_i^N \omega_i I_{iz} + \sum_{i,j}^N D_{ij} I_{iz} I_{jz} \tag{11.20}$$

where D_{ij} is the internuclear dipolar interaction, as defined in eqns 3.76 and 4.53, and given by

$$\begin{aligned} D_{ij} &= \frac{\mu_0 \gamma^2 \hbar}{4\pi} \frac{1}{r_{ij}^3} \frac{1}{2} (1 - 3\cos^2\theta_{ij}) 3 I_{iz} I_{jz} \\ &= 3\omega_{ij} I_{iz} I_{jz} \end{aligned} \tag{11.21}$$

Equation 11.21 does not include all secular terms from the dipolar interaction Hamiltonian, but only the $I_{iz}I_{jz}$ associated with the formation of multiple echoes. Notice that conventionally we neglect these terms. In solids the sum of dipolar coupling terms for the i-th spin is generally 10^4 smaller than the Zeeman term, and in liquids some further 10^4 lower due to motional averaging. Thus dipolar interactions are usually ignored as far as the composition of the equilibrium density matrix is concerned, and it is generally sufficient to use a single-spin picture when calculating the equilibrium magnetisation. But when considering the sum of all possible intermolecular dipolar interactions, and especially at high polarising fields, this assumption requires closer examination.

In a single-spin picture, we would write the thermal equilibrium density matrix in the HTA as

$$\sigma_{eq} \approx \tfrac{1}{2} \left(\mathbf{1} + \beta\omega_i I_{iz}\right) \tag{11.22}$$

Hence for an N spin system, the density matrix becomes

$$\begin{aligned} \rho_{eq} &= \sigma_{1eq} \otimes \sigma_{2eq} \otimes \sigma_{3eq} \ldots\ldots \otimes \sigma_{Neq} \\ &= 2^{-N} \Pi_i \left(\mathbf{1} + \beta\omega_i I_{iz}\right) \end{aligned} \tag{11.23}$$

This product involves N one-spin operators on the order of size $\gamma B_0/k_BT$, $N^2/2$ two-spin operators (on the order of size $(\gamma B_0/k_BT)^2$), and higher-order spin operators in succession. Despite the fact that $\gamma B_0/k_BT \sim 10^{-4}$ for protons at 10-T field strengths, the increasing multiplicity of higher-order terms by successive powers of N means that higher-order terms in the density matrix cannot be ignored without some further justification.

Conventionally we justify ignoring bilinear terms in the density matrix by the fact that all subsequent Zeeman interactions produce density matrix terms that remain

bilinear and so cannot result in the NMR observables I_x or I_y. But the dipolar field introduces bilinear Hamiltonian terms that are capable of generating observable coherences from higher-order density matrix elements. Here we might argue that molecular self diffusion will cause such interactions to fluctuate and therefore average to zero, but this argument can only hold for spins that are in close proximity. Beyond some characteristic distance, such Brownian motion will not suffice, as we will see. Finally, we might hope that the $1/r^3$ dependence of D_{ij} would render the effect of distant spins insignificant. In fact this is not the case, especially when asymmetry of the surrounding dipolar magnetisation allows for a significant integral effect. Such asymmetry will always play a significant role when magnetic field gradients are used, and so these dipolar effects become of particular importance in PGSE NMR and NMR imaging.

Beyond the 'diffusion sphere'

Consider two particles, labelled 1 and 2, which migrate via Brownian motion over some fixed time, as illustrated in Fig. 11.12. If the particles are proximate, their internuclear vectors can undergo a significant reorientation due to the relative Brownian motion as seen in (a). In (b), where the spins are more distant, the same relative translational motion leads to a minor change in interparticle vector orientation, thus making motional averaging of the dipolar interaction much less likely. As pointed out by Warren *et al.*, molecular self-diffusion in liquids causes dipolar interactions to be averaged to zero for spins on nearby molecules, but beyond a diffusion length corresponding to

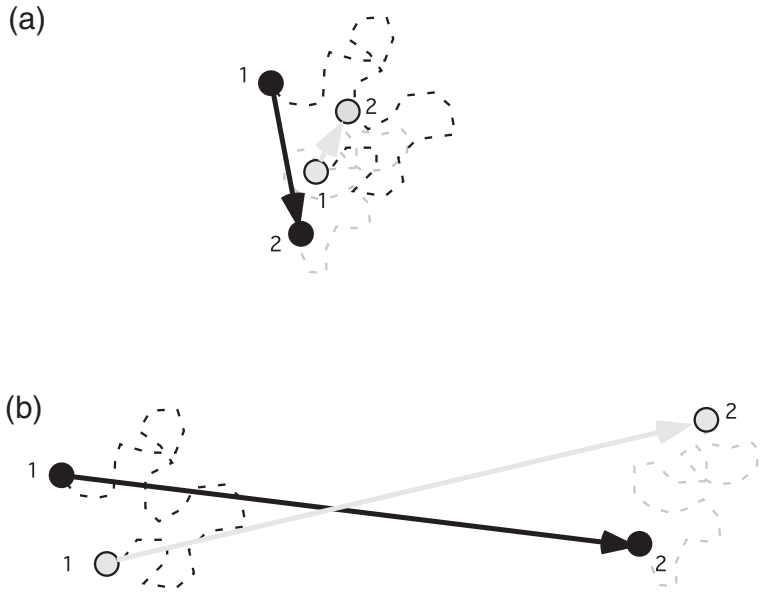

Fig. 11.12 (a) Proximate particles, 1 and 2, undergoing relative Brownian motion over some fixed time interval. (b) The same relative Brownian motion but for distant particles. Here the interparticle vectors reorient much less significantly.

the characteristic NMR timescale such averaging does not apply. That length is easily calculated by finding the distance such that the dipolar interaction strength in hertz at that spin separation equates to the inverse time required to diffuse that distance. For pairs of protons in water, the dipolar interaction strength at about 0.5 nm separation is on the order of 500 Hz, while the diffusion time for 0.5 nm is around 6×10^{-11} s, so that there is no doubt that the dipolar interaction is motionally averaged to zero by diffusion. At greater distances, as the pairwise dipolar interaction decreases as r^{-3}, while the diffusion time grows as r^2, strict motionally averaging requirements are even more strongly observed. But what makes the long-range intermolecular dipolar contribution behave differently than the simple two-spin picture is the sum of contribution from N spins. What counts therefore is the characteristic time associated with the dipolar field generated by the sample nuclear magnetisation, M_{eq}. This magnetic field strength is $\mu_0 M_{eq}$, and so the characteristic precession time for spin i in this field is $\tau_d = (\gamma \mu_0 M_{eq})^{-1}$. The equilibrium nuclear magnetisation is given in eqn 3.89 and for water protons at 300 K and 14.1 T (600 MHz) $M_{eq} = 0.045\,\mathrm{JT^{-1}m^{-3}}$ and $\tau_d = 0.066$ s. The characteristic water molecule diffusion length for this time is thus on the order of 10 microns and within this length motional averaging caused by translational diffusion is effective.

Beyond that diffusion sphere radius, dipolar contributions from remote spins do contribute to the field experienced by any spin within that sphere, and the volume integral of $r^2 dr$ r over the r^{-3} dependence of the dipolar interaction ensures a logarithmic contribution, the magnitude of which depends on the ratio of the sample dimension to the diffusion length.

For spherical samples the angular dependence of the dipolar interaction in the integral contribution from all spins ensures that the sum of the dipolar field vanishes. However, if the spherical symmetry is broken, for example by application of a magnetic field gradient, then the effects of the dipolar field will be felt by the spins and the conversion of higher-order coherences into observable magnetisation becomes possible.

11.3.2 Multi-echo and CRAZED phenomena

Figure 11.13 shows two versions of a simple two 90° RF pulse sequence. The first involves a steady background gradient and the second is a two-dimensional multiple-quantum experiment, with independent time domains t_1 and t_2, using pulsed gradients of differing time interval to select for higher-order coherence in the evolution period t_1. This latter sequence we met earlier in the CRAZED experiment.

The generation of the observables

Let us begin by trying to understand the multi-echoes using the quantum mechanical density matrix approach. We can begin by stating the obvious: thermal equilibrium density matrix terms linear in I_z contribute to a primary echo at $t_2 = t_1$. So let us see how the gradient and dipolar interactions combine with density matrix terms bilinear in I_z to play a role in making multiple echoes possible. Ignoring the effects of spin–spin relaxation, we start by considering the evolution of an element of the second-order term $(\gamma B_0 / k_B T)^2 I_{iz} I_{jz}$, arising in the equilibrium density matrix, ρ_{eq}.

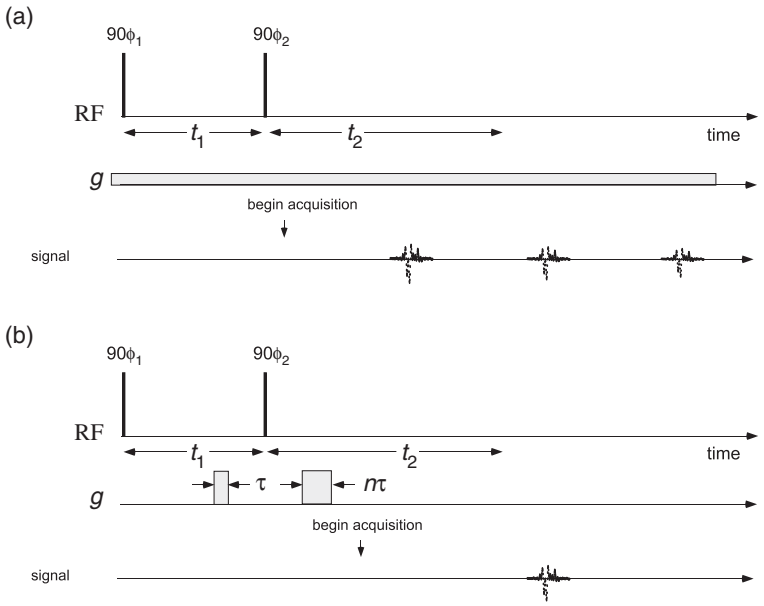

Fig. 11.13 (a) Pulse sequence for demonstrating the multiple spin-echo effect due to intermolecular dipolar interactions experiment. ϕ_1 and ϕ_2 denote the phase of the RF pulses. g is a steady background gradient in the z direction unless otherwise stated. The multiple spin-echo signals occur at $t_2 = t_1$, $t_2 = 2t_1$, $t_2 = 3t_1 \ldots$ (b) The nth-order CRAZED experiment [3], in which homospoil gradient pulses of different area can be used to select specific echoes according to their n quantum origin during the period t_1. τ is the period of the first gradient pulse, n is an integer multiple, and the the CRAZED signal occurs at $t_2 = nt_1$. (Adapted from Minot *et al.* [28].)

To clearly distinguish the Larmor and dipolar precessions, we use the symbols ω_i and D_{ij}, respectively, noting that the dipolar interaction causes I_{iy} to evolve to $\cos(\frac{1}{2}D_{ij}t)I_{iy} + \sin(\frac{1}{2}D_{ij}t)I_{ix}I_{jz}$, while the Larmor precession takes I_{iy} to $\cos(\omega_i t)I_{iy} + \sin(\omega_i t)I_{ix}$. For the moment, we will allow that the Larmor precession may be associated with the intrinsic chemical shift of the spin where a molecular mixture exists, as well as from the local position in a magnetic field gradient.

The first 90°_x pulse converts $I_{iz}I_{jz}$ to $I_{iy}I_{jy}$, then via the Zeeman and dipolar interactions to

$$\begin{aligned}\rho(t_{1-}) = \cos^2(\tfrac{1}{2}D_{ij}t_1)[&I_{iy}I_{jy}\cos(\omega_i t_1)\cos(\omega_j t_1) + I_{ix}I_{jy}\sin(\omega_i t_1)\cos(\omega_j t_1)\\ &+I_{iy}I_{jx}\cos(\omega_i t_1)\sin(\omega_j t_1) + I_{ix}I_{jx}\sin(\omega_i t_1)\sin(\omega_j t_1)]\\ &+\sin(\tfrac{1}{2}D_{ij}t_1)\cos(\tfrac{1}{2}D_{ij}t_1)[2I_{ix}I_{jz}I_{jy}\cos(\omega_i t_1)\cos(\omega_j t_1)\\ &-2I_{iy}I_{jz}I_{jy}\sin(\omega_i t_1)\cos(\omega_j t_1)\\ &+2I_{ix}I_{jz}I_{jx}\cos(\omega_i t_1)\sin(\omega_j t_1) - 2I_{iy}I_{jz}I_{jx}\sin(\omega_i t_1)\sin(\omega_j t_1)]\ldots\end{aligned} \tag{11.24}$$

Since the intermolecular dipolar interaction is weak, and $D_{ij}t_1, D_{ij}t_2 \ll 1$, only terms involving one $\sin(\frac{1}{2}D_{ij}t_2)$ factor need be considered as making any significant contribution to the signal.

Following the second 90°_x RF pulse the density matrix becomes

$$\begin{aligned}\rho(t_{1+}) = \cos^2(\tfrac{1}{2}D_{ij}t_1)[&I_{iz}I_{jz}\cos(\omega_i t_1)\cos(\omega_j t_1) + I_{ix}I_{jz}\sin(\omega_i t_1)\cos(\omega_j t_1)\\ &+I_{iz}I_{jx}\cos(\omega_i t_1)\sin(\omega_j t_1) + I_{ix}I_{jx}\sin(\omega_i t_1)\sin(\omega_j t_1)]\\ &-\sin(\tfrac{1}{2}D_{ij}t_1)\cos(\tfrac{1}{2}D_{ij}t_1)[-2I_{ix}I_{jy}I_{jz}\cos(\omega_i t_1)\cos(\omega_j t_1)\\ &+2I_{iz}I_{jy}I_{jz}\sin(\omega_i t_1)\cos(\omega_j t_1)\\ &-2I_{ix}I_{jy}I_{jx}\cos(\omega_i t_1)\sin(\omega_j t_1) + 2I_{iz}I_{jy}I_{jx}\sin(\omega_i t_1)\sin(\omega_j t_1)]... \quad (11.25)\end{aligned}$$

Subsequently, over the period t_2, the density matrix evolves to over 100 different terms. However, the only terms capable of generating observable magnetisation under the influence of the dipolar interaction are those involving products such as $I_{ix}[I_{jz}I_{jz}...]$ or $I_{iy}[I_{jz}I_{jz}...]$. Terms involving $I_{ix}I_{jz}I_{jz}$ will generate $n = 3$ echoes, $I_{ix}I_{jz}I_{jz}I_{jz}$, $n = 4$ and so on. Let us focus on $n = 2$. For example, consider the term $\cos^2(\frac{1}{2}D_{ij}t_1)I_{ix}I_{jz}\sin(\omega_i t_1)\cos(\omega_j t_1)$ in eqn 11.25. Under the dipolar interaction and the Larmor precessions it evolves during t_2 to

$$\begin{aligned}\rho_{visible}(t_1,t_2) = \sum_{i=1}^{N}\sum_{j=1}^{N}&\sin(\tfrac{1}{2}D_{ij}t_2)\cos^2(\tfrac{1}{2}D_{ij}t_1)[I_{iy}\sin(\omega_i t_1)\cos(\omega_j t_1)\cos(\omega_i t_2)\\ &+I_{ix}\sin(\omega_i t_1)\cos(\omega_j t_1)\sin(\omega_i t_2)] \quad (11.26)\end{aligned}$$

To identify the relevant precession frequencies of contributing terms, the products of sines and cosines need to be factorised in terms of sum and difference frequencies $\omega_i + \omega_j$ and $\omega_i - \omega_j$.

The magnetic field gradient and nuclei with common chemical shift

Suppose we have a sample of a common molecular species—for simplicity, one with a single chemical shift, such as water or polydimethylsiloxane, such that Larmor frequency differences are entirely due to applied magnetic field gradients. What we seek is an understanding of how the $n = 2$ echo arises (and by implication all higher-order echoes) and what will govern its amplitude. To appreciate the role of the applied magnetic field gradient, we allow that the Larmor frequencies ω_i and ω_j arise from the different locations of spins i and j. For a gradient g directed along an axis s, then spin i at position s_i will have a Larmor frequency $\omega_i = \gamma(B_0 + gs_i)$. Signal from transverse magnetisation terms in eqn 11.26, modulated by sinusoidal functions of absolute position, $\sin(\omega_i + \omega_j)t$ or $\cos(\omega_i + \omega_j)t$, will be averaged to zero. Also averaged to zero will be odd functions of relative position $\sin(\omega_i - \omega_j)t$. By contrast, signal from terms modulated by even functions of relative position, $\cos(\omega_i - \omega_j)t) = \cos\gamma g(s_i - s_j)t$, will not average to zero because the coefficient $D_{ij}t_2$ introduces the factor r_{ij}^{-3}, thus giving the sinusoids a decay envelope that ensures that even functions of relative position have a non-zero integral over the sample space.

The subtlety of the multiple-quantum coherences

At first sight, the precession rate during the t_1 period of the signal-contributing term in eqn 11.26 appears to involve a double-quantum coherence $I_{ix}I_{jy}$, whereas during the t_2 period the term precesses as a single-quantum coherence. This alone would suggest the need for a factor of two difference in gradient time integrals in the t_1 and t_2 periods if an echo is to be formed. In truth, the matter is a little more subtle. Unlike the case for scalar coupled spins, the intermolecular dipolar interaction means that spins i and j are at very different locations and have very different Larmor frequencies in the presence of the gradient. It is in the decomposition of the $\sin(\omega_i t_1)\cos(\omega_j t_1)\sin(\omega_i t_2)$ factor, and the requirement that the signal arises only from terms modulated by even functions of relative position, that the relationship between t_2 and t_1 is set. For the constant gradient experiment, as in Fig. 11.13(a), this means that a $\frac{1}{4}\cos(\omega_i t_1 + \omega_j t_1 - \omega_j t_2)$ term reduces to the required 'slow'-oscillatory $\cos(\omega_i - \omega_j)t_1$ form when $t_2 = 2t_1$.

CRAZED

CRAZED is a two-dimensional experiment where t_1 and t_2 are independently varied, and we need to allow that the separate effect of different chemical shifts (say ω_{0i} and ω_{0j}) in the molecular mixture is accounted for, as well as the effect of the homospoil gradient pulses. Allowing for both gradients and chemical shift, now our $\frac{1}{4}\cos(\omega_i t_1 + \omega_j t_1 - \omega_j t_2)$ term decomposes and factorises (keeping only the terms modulated by even functions of relative position), as

$$\begin{aligned}\cos(\omega_i t_1 + \omega_j t_1 - \omega_j t_2) &= \cos(\omega_{0i} t_1 + \omega_{0j} t_1 + \gamma g s_i \tau + \gamma g s_j \tau - \omega_{0j} t_2 - \gamma g s_j 2\tau) \\ &= \cos\left(\omega_{0i} t_1 + \omega_{0j} t_1 - \omega_{0j} t_2 + \gamma g (s_i - s_j)\tau\right) \\ &\rightarrow \cos(\omega_{0i} t_1 + \omega_{0j} t_1)\cos(\omega_{0j} t_2)\cos\left(\gamma g (s_i - s_j)\tau\right)\end{aligned} \tag{11.27}$$

And, of course, similar terms arise with ω_{0i} as the frequency in the t_2 dimension. The final factor governs the signal amplitude in the t_2 domain, and has required the factor of two difference in gradient pulse area. It is just as the condition for a double-quantum coherence experiment, but with the subtlety of a maximum formed by integration of a slowly oscillatory phase factor over macroscopic sample dimensions, rather than a simple phase cancellation. For the chemical shift locations in the f_1 dimension, the sum of molecular chemical shifts arises, exactly as seen in Fig. 11.11, while in the acquisition, f_2 dimension, single frequency oscillation occurs. The resemblance to a double-quantum COSY experiment is compelling. But underlying this effect are not single-spin operators, but pseudo-density matrix operators made up of macroscopic ensemble averages.

The intermolecular integral and gradient symmetry breaking

Now we are in a position to calculate the total contribution to the higher-order signal components represented by the visible terms from eqn 11.26 that emerge with gradient phase modulation and dipolar amplitude as $I_{xi}\cos(\gamma g t_1 (s_i - s_j) D_{ij} t_2$. Suppose we integrate these contributions over the entire sample outside the diffusion sphere around spin i. Then the contribution will be determined by the factor

$$\int_{volume} \cos(\gamma g t_1 \mathbf{r} \cdot \hat{\mathbf{s}}) \frac{3\cos^2\theta - 1}{r^3} r^2 \sin\theta d\theta d\phi dr \tag{11.28}$$

where $\hat{\mathbf{s}}$ is the unit vector describing the gradient direction, and $\mathbf{r}$ defines the position of the remote spin in polar coordinates, where θ is taken with respect to the polarising field direction, $\hat{\mathbf{z}}$. The term $(3\cos^2\theta - 1)/r^3$ introduces the spatial dependence of D_{ij}. It can be shown [1] that eqn 11.28 reduces to

$$[3(\hat{\mathbf{s}} \cdot \hat{\mathbf{z}})^2 - 1] \int_{r_{min}} F(\gamma g t_1 r) dr \tag{11.29}$$

where the function F contains all r dependence, and has an integral that is greatest when $\gamma g t_1 r$ ranges between two and four in a large fraction of the sample, i.e. when the gradient imparts to the spins a helical phase twist with wavelength smaller than the sample dimensions but larger than the diffusion radius, r_{min}.

11.3.3 Experimental verification of multiple echo effect

The smaller the diffusion radius, r_{min}, the larger the integral of F. Hence larger multi-order echoes from intermolecular dipolar effects are observed for more slowly diffusing liquids. Figure 11.14 shows the results obtained using a sample of 5000-Da polydimethylsiloxane at 7 T polarising field strength [28]. Echoes out to order four are clearly visible. The phases of the higher-order echoes vary, in a predictable manner, according to the density matrix terms from which they originate.

Figure 11.15 shows the result of the CRAZED 'multi-quantum' experiment where homospoil gradient pulses are used to select for echo order, according to the value n chosen for the ratio of the gradient pulse integral during t_2 to that of the period t_1. Note that specific echo orders can also be selected by appropriate phase cycling, and examples of these cycles up to $n = 3$ are given in reference [28].

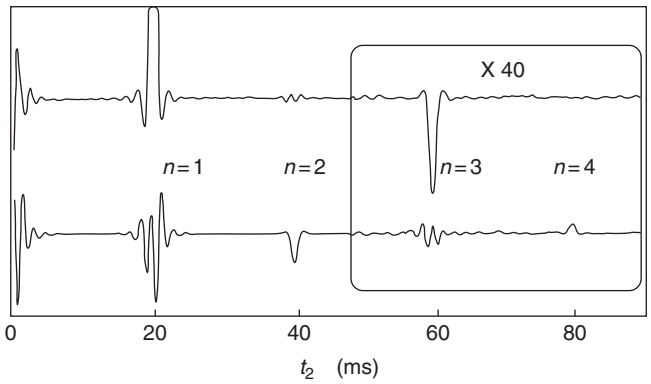

Fig. 11.14 Time-domain signals from the multi-echo experiment with steady gradient (Fig. 11.13(a)) where $\phi_1 = \phi_2 = x$ and $g = 0.04\,\mathrm{mT\,m^{-1}}$. The upper line is the imaginary channel and the lower line is the real channel. Data within the box are magnified 40 times. (Adapted from Minot *et al.* [28].)

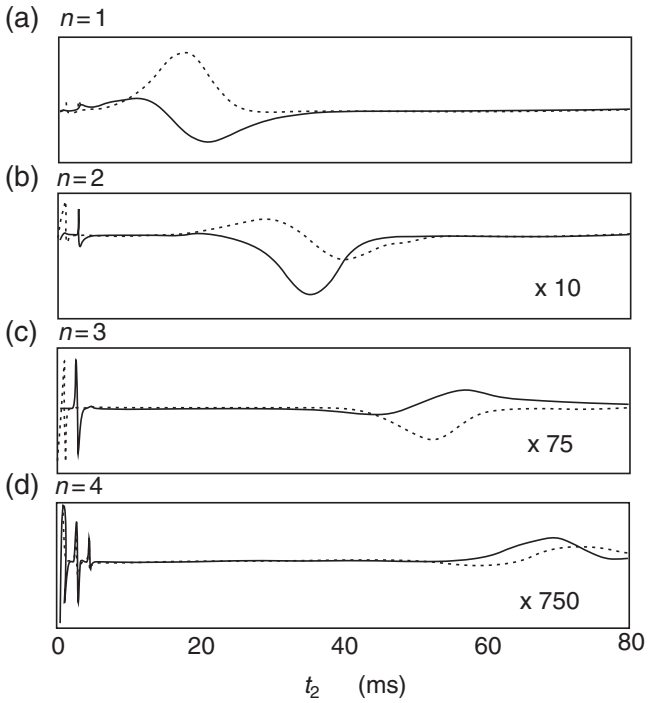

Fig. 11.15 Time-domain signals from the nth order multi-echo (CRAZED) experiment, with pulsed gradient (Fig. 11.13(b)). The solid lines show the real channel data and the dashed lines show the imaginary channel. Magnification relative to (a) is shown in (b) to (d). Here $\phi_1 = \phi_2 = x$, $t_1 = 20\,\text{ms}$ and the gradient duration τ is 2 ms. (Adapted from Minot *et al.* [28].)

Note the role of the factor $[3(\hat{\mathbf{s}}\cdot\hat{\mathbf{z}})^2 - 1]$. Changing the applied gradient direction from $\hat{\mathbf{z}}$ to one transverse to $\hat{\mathbf{z}}$ changes the sign of the echo. And of course, when $\hat{\mathbf{s}}\cdot\hat{\mathbf{z}} = 1/3$, in other words when the gradient direction is set to the magic angle $\theta = 54.4°$, the symmetry-breaking effect of the gradient disappears and any intermolecular dipolar echoes must arise from sample shape alone. Here the damping effect in the integral of F ensures that sample shape will not contribute to the formation of multi-echoes, provided the sample size is much larger than the gradient-induced wavelength. By this means, it is possible to avoid the appearance of unwanted intermolecular dipolar echos in PGSE NMR experiments by using a sufficiently large homospoil gradient oriented at the magic angle.

11.3.4 Probing structure via intermolecular coherences

The role of the function F in determining the amplitude of the higher-order echo signal suggests a possible use in structural determination [29–32]. Returning to eqn 11.28, we can see that it assumes a uniform sample magnetisation modulated in phase by the applied gradient. Suppose instead we allowed for a more general contribution of

magnetisation phase and amplitude which depended on sample structure. In that case, we need to rewrite the integral allowing for the sample density $\rho(\mathbf{r})$ at the origin of the i spin and $\rho(\mathbf{r}')$ at the remote j spin, separately integrating each set of coordinates. Hence we could rewrite eqn 11.28 as

$$\int_{volume} d\mathbf{r}d\mathbf{r}'\rho(\mathbf{r})\rho(\mathbf{r}')\cos(\gamma g t_1(\mathbf{r}-\mathbf{r}')\cdot\hat{\mathbf{s}})\frac{3\cos^2\theta_{rr'}-1}{|\mathbf{r}-\mathbf{r}'|^3} \tag{11.30}$$

By adjusting the spatial period of the gradient-induced phase shift, the higher-order echo signal can be used to probe correlations in structure $\rho(\mathbf{r})$ and $\rho(\mathbf{r}')$ at differing spatial separations, $\mathbf{r}-\mathbf{r}'$. The inverse problem to be solved is not trivial, but the potential advantage of the method is that, unlike conventional NMR microscopy, the entire sample contributes to the signal, as the resolution is improved by increasing the gradient wavevector, thus maintaining high signal-to-noise ratio. However, the lower limit to resolution is still constrained by the diffusion sphere, and so in aqueous systems, is around 10 microns.

The theoretical description and mathematical details of the problem are complex, though somewhat assisted by working in the Fourier space of $\mathbf{r}$, in which case expression 11.30 can be written in terms of overlap integrals. Complementary treatments of the problem are described in detail in references [31] and [29]. While the method clearly has some potential, the connection between sample structure and the gradient wavevector-dependent multi-echo signal is not particularly transparent. However, it can be useful in demonstrating structural anisotropy in a porous material [31].

References

[1] G. Deville, M. Bernier, and J. M. Delrieux. NMR multiple echoes observed in solid 3-He. *Phys. Rev. B*, 19:5666, 1979.

[2] M. A. McCoy and W. S. Warren. 3-quantum nuclear magnetic resonance spectroscopy of liquid water-intermolecular multiple quantum coherence generated by spin cavity coupling. *J. Chem. Phys.*, 93:858, 1990.

[3] Q. H. He, W. Richter, S. Vathyam, and W. S. Warren. Intermolecular multiple-quantum coherences and cross correlations in solution nuclear magnetic resonance. *J. Chem. Phys.*, 98:6779, 1993.

[4] W. S. Warren, W. Richter, A. H. Andreotti, and B. T. Farmer. Generation of impossible cross-peaks between bulk water and biomlecules in solution NMR. *Science*, 262:2005, 1993.

[5] W. S. Warren, S. Lee, W. Richter, and S. Vathyam. Correcting the classical dipolar demagnetizing field in solution NMR. *Chemical Physics Letters*, 247:207, 1995.

[6] S. Lee, W. Richter, S. Vathyam, and W. S. Warren. Quantum treatment of the effects of dipole-dipole interactions in liquid nuclear magnetic resonance. *J. Chem. Phys.*, 105:874, 1996.

[7] W. Richter and W. S. Warren. Intermolecular multiple quantum coherences in liquids. *Concepts in Magnetic Resonance*, 12:396, 2000.

[8] J. F. Martin, L. S. Selwyn, R. R. Void, and R. L. Void. The determination of translational diffusion constants in liquid crystals from pulsed field gradient double quantum spin echo decays. *J. Chem. Phys.*, 76:2632, 1982.

[9] D. Zax and A. Pines. Study of anisotropic diffusion of oriented molecules by multiple quantum spin echoes. *J. Chem. Phys.*, 78:6333, 1983.
[10] G. Bodenhausen, R. R. Void, and R. L. Void. Multiple quantum spin-echo spectroscopy. *J. Magn. Reson.*, 37:93, 1980.
[11] G. J. Bowden, W. D. Hutchison, and J. Kachan. Tensor operator formalism for multiple quantum NMR. I. Spin-1 nuclei. *Molecular Physics*, 67:415, 1986.
[12] L. van Dam, B. Andreasson, and L. Nordenskiold. Multiple-quantum pulsed gradient NMR diffusion experiments on quadrupolar ($i > 1/2$) spins. *Chemical Physics Letters*, 262:737, 1996.
[13] L. E. Kay and J. H. Prestegard. An application of pulse-gradient double-quantum spin echoes to diffusion measurements on molecules with scalar-coupled spins. *J. Magn. Reson.*, 67:103, 1986.
[14] P. W. Kuchel and B. E. Chapman. Heteronucelar double quantum coherence selection with magnetic field gradients in diffusion experiments. *J. Magn. Reson.*, A101:53, 1993.
[15] A. J. Dingley, J. P. Mackay, G. L. Shaw, B. D. Hambly, and G. F. King. Measuring macromolecular diffusion using heteronuclear multiple-quantum pulsed-field-gradient NMR. *Journal of Biomolecular NMR*, 10:1, 1997.
[16] M. R. Bendall, D. T. Pegg, D.M. Doddrell, and J. Field. Inverse DEPT sequence. Polarization transfer from a spin-1/2 nucleus to n spin-1/2 heteronuclei via correlated motion in the doubly rotating reference frame. *J Magn. Reson.*, 51:520, 1983.
[17] K. I. Momot and P. W. Kuchel. Convection-compensating diffusion experiments with phase-sensitive double-quantum filtering. *J. Magn. Reson.*, 574:229, 2005.
[18] G. Zheng, A. M. Torres, and W. S. Price. MQ-PGSTE: A new multi-quantum STE-based PGSE NMR sequence. *J. Magn. Reson.*, 198:271, 2010.
[19] S. Cavadini and P. R. Vasos. Singlet states open the way to longer time-scales in the measurement of diffusion by NMR spectroscopy. *Concepts in Magnetic Resonance*, 32A:68, 2008.
[20] M. Carravetta, O. G. Johannessen, and M. H. Levitt. Beyond the T_1 limit: singlet nuclear spin states in low magnetic fields. *Phys. Rev. Lett.*, 92:153003–1, 2004.
[21] M. Carravetta and M. H. Levitt. Long-lived nuclear spin states in high-field solution NMR. *J. Am. Chem. Soc.*, 126:6228, 2005.
[22] M. Carravetta and M. H. Levitt. Theory of long-lived nuclear spin states in solution nuclear magnetic resonance. *J. Chem. Phys.*, 122:214505, 2005.
[23] S. Cavadini, J. Dittmer, S. Antonijevic, and G. Bodenhausen. Slow diffusion by singlet state NMR spectroscopy. *J. Am. Chem. Soc.*, 127:15744, 2005.
[24] N. N. Yadav, A. M. Torres, and W. S. Price. q-space imaging of macroscopic pores using singlet spin states. *J. Magn. Reson.*, 234:306, 2010.
[25] A. Abragam. *Principles of Nuclear Magnetism*. Clarendon Press, Oxford, 1961.
[26] J. Jeener, A. Vlassenbroek, and P. Broekaert. Unified derivation of the dipolar field and relaxation terms in the bloch-redfield equations of liquid NMR. *J. Chem. Phys.*, 103:1309, 1995.
[27] M. H. Levitt. Demagnetization field effects in two-dimensional solution NMR. *Concepts Magn. Reson.*, 8:77, 1996.

[28] E. D. Minot, P. T. Callaghan, and N. Kaplan. Multiple echoes, multiple quantum coherence, and the dipolar field: Demonstrating the significance of higher order terms in the equilibrium density matrix. *J. Magn. Reson.*, 140:200, 1999.

[29] R. Bowtell and P. Robyr. Structural investigations with the dipolar demagnetizing field in solution NMR. *Phys. Rev. Lett..*, 76:4971, 1996.

[30] R. Bowtell and P. Robyr. Nuclear magnetic resonance microscopy in liquids using the dipolar field. *J. Chem. Phys.*, 10:467, 1997.

[31] L. S. Bouchard and W. S. Warren. Reconstruction of porous material geometry by stochastic optimization based on bulk NMR measurements of the dipolar field. *J. Magn. Reson.*, 170:299, 2005.

[32] L.S. Bouchard, F. W. Wehrli, C.L. Chin, and W.S. Warren. Structural anisotropy and internal magnetic fields in trabecular bone: Coupling solution and solid dipolar interactions. *J. Magn. Reson.*, 176:27, 2005.